Cell

Microbial transformation of dietary xenobiotics shapes gut microbiome composition

Graphical abstract

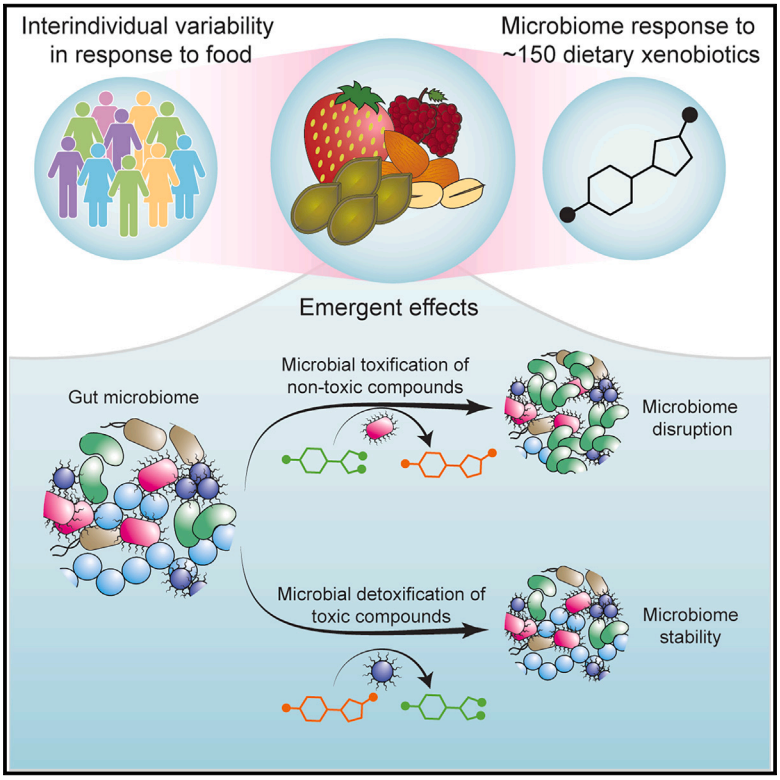

Authors

Elizabeth J. Culp, Nora T. Nelson, Andrew A. Verdegaal, Andrew L. Goodman

Correspondence

andrew.goodman@yale.edu

In brief

Individuals can exhibit significant interpersonal variation in diet-microbiome interaction. This report uncovers how gut microbes can convert some dietary compounds into antibiotics and detoxify others, highlighting mechanisms that explain why the same dietary compound can have different effects on the microbiomes of different individuals.

Highlights

- Mapping interactions between the microbiome and ~150 dietary xenobiotics
- Microbial metabolism can convert some compounds into antibiotics and detoxify others
- Identification of enzymes that determine community remodeling by dietary xenobiotics

Culp et al., 2024, Cell *187*, 6327–6345
October 31, 2024 © 2024 Elsevier Inc. All rights are reserved, including those for text and data mining, AI training, and similar technologies.
https://doi.org/10.1016/j.cell.2024.08.038

CellPress

Cell

CellPress

Article

Microbial transformation of dietary xenobiotics shapes gut microbiome composition

Elizabeth J. Culp,[1] Nora T. Nelson,[1,2] Andrew A. Verdegaal,[1,2] and Andrew L. Goodman[1,3,*]
[1]Department of Microbial Pathogenesis and Microbial Sciences Institute, Yale University School of Medicine, New Haven, CT, USA
[2]These authors contributed equally
[3]Lead contact
*Correspondence: andrew.goodman@yale.edu
https://doi.org/10.1016/j.cell.2024.08.038

SUMMARY

Diet is a major determinant of gut microbiome composition, and variation in diet-microbiome interactions may contribute to variation in their health consequences. To mechanistically understand these relationships, here we map interactions between ~150 small-molecule dietary xenobiotics and the gut microbiome, including the impacts of these compounds on community composition, the metabolic activities of human gut microbes on dietary xenobiotics, and interindividual variation in these traits. Microbial metabolism can toxify and detoxify these compounds, producing emergent interactions that explain community-specific remodeling by dietary xenobiotics. We identify the gene and enzyme responsible for detoxification of one such dietary xenobiotic, resveratrol, and demonstrate that this enzyme contributes to interindividual variation in community remodeling by resveratrol. Together, these results systematically map interactions between dietary xenobiotics and the gut microbiome and connect toxification and detoxification to interpersonal differences in microbiome response to diet.

INTRODUCTION

The human microbiome has wide-ranging impacts on our health. Each individual hosts trillions of commensal microbes that vary widely between people and collectively encode over 150 times more genes than the human genome.[1] The genetic and metabolic capability of these bacteria provide functions essential to maintaining a healthy state, while microbiome dysbiosis can contribute to diseases including cardiovascular disease,[2,3] inflammatory bowel diseases,[4] type 2 diabetes,[5] obesity,[6] and cancer.[7] However, with few exceptions, the mechanisms by which the microbiome contributes to health are poorly understood.

Diet is another clear contributor to health. It is thus somewhat surprising that epidemiological evidence for the health impacts of individual biochemicals contained in food (dietary xenobiotics) is limited. These equivocal results can be highlighted in the context of cancer, where up to 35% of disease risk is attributable to diet, but evidence for specific foods responsible for cancer risk has been largely elusive.[8] Similarly, there is limited efficacy for controlling metabolic syndromes such as type 2 diabetes using dietary recommendations that are based on population averages.[9] Indeed, human subjects experience significant interindividual variability in their responses to the same food,[10] for example, as quantified in postprandial metabolic measures.[11] Person-specific factors such as the microbiome may represent an important component of this variability, which is sometimes overlooked in studies evaluating links between diet and health.[9,11]

The gut microbiome interacts closely with dietary xenobiotics, and diet is a major determinant of gut microbiome composition.[12–15] Previous research on how diet shapes the gut microbiome has largely focused on macronutrients (fats,[16] proteins,[17] and carbohydrates[18]), particularly plant polysaccharides that escape human digestive enzymes and act as an important energy source for bacteria in the colon.[18–20] Notably, studies focused on macronutrient intake suggest that dietary manipulation represents a tractable means to manipulate the gut microbiome.[11,21] Gut microbes also have a robust capacity to metabolize dietary macronutrients, which results in increased energy harvest for the host[22] and the production of bioactive metabolites such as fatty acids (short chained, branched chain, and aromatic) and amines.[18,23]

In addition to macronutrients, our diets contain an enormous biochemical complexity of micronutrients, encompassing >26,000 unique dietary xenobiotics, including polyphenols, lignans, stilbenes, and tannins.[24,25] Previous research on these compounds illustrates their potential to contribute toward host health[26,27] and impact microbiome composition.[28–31] For a small number of dietary xenobiotics, microbial metabolism has been shown to modulate their impact on health and disease.[2,32,33] However, apart from these examples, most previous research has focused on mixtures or whole foods rather than pure compounds, provides aggregated measurements that mask

All rights are reserved, including those for text and data mining, AI training, and similar technologies.

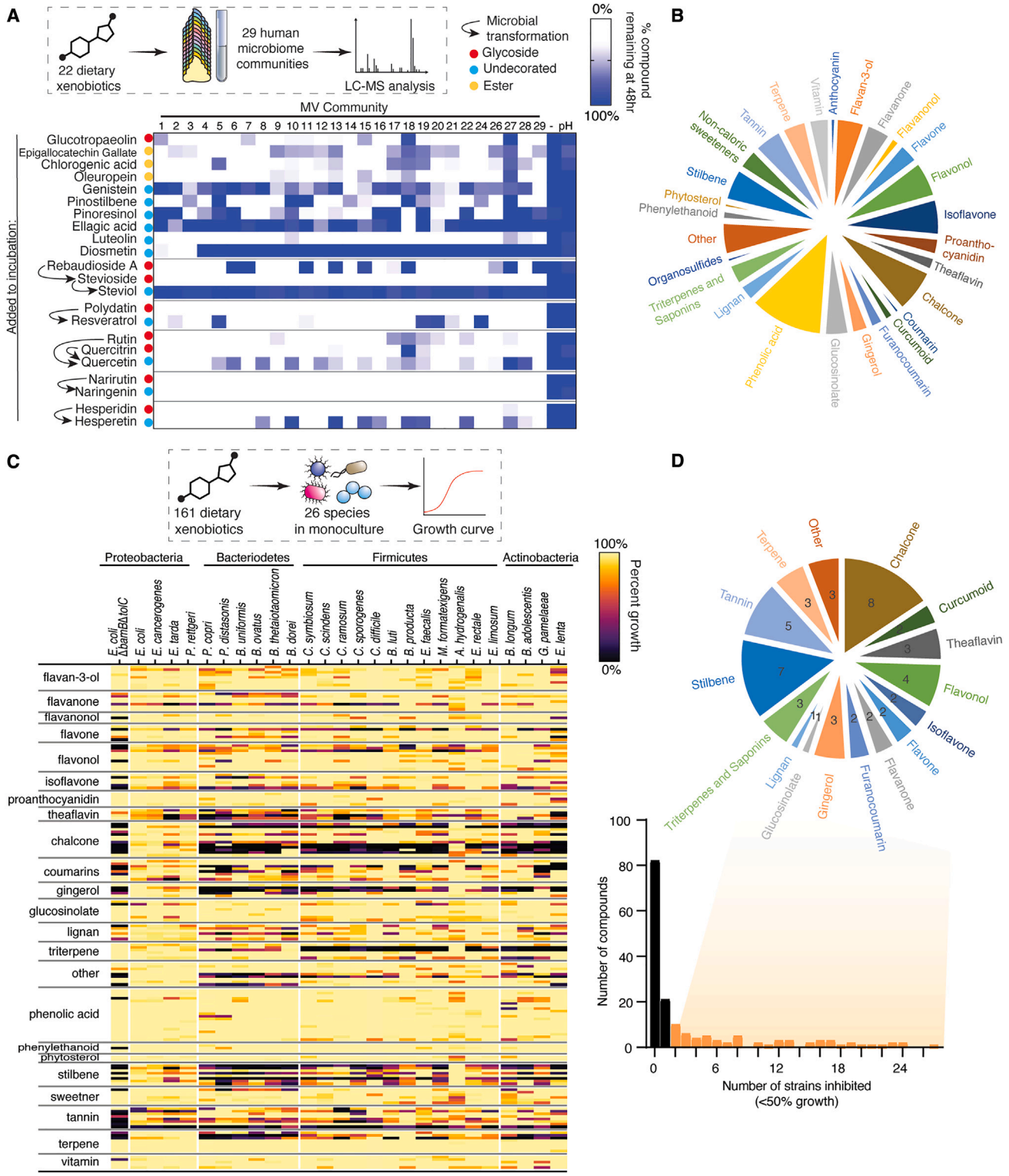

Figure 1. Dietary xenobiotics are variably metabolized by gut microbiome communities and can inhibit growth of gut commensals

(A) *Ex vivo* incubation of 29 human fecal samples (MV collection), plus a pH 5 control, with 22 dietary xenobiotics and their metabolites illustrates interindividual variability in compound metabolism. Levels of each compound after incubation with each community at 10–20 μM were determined by LC-MS and normalized to ion abundance in sterile media controls ("-"). Compounds related through microbial transformation are indicated by arrows. Mean of triplicate incubations is shown. A pH 5 control is also indicated.

(legend continued on next page)

interindividual variability, or relied on animal models that may not capture the metabolic potential of human microbiomes.

Studies of microbiome interactions with small-molecule medical drugs reveal a broad capacity of these drugs to alter microbial growth,[34] highlight extensive and variable microbial metabolism,[35,36] and provide examples of microbiome contributions to interindividual variability in drug efficacy and toxicity.[36,37] Similarly, interindividual variability in the response to diet may result from variability in the microbial metabolites produced from dietary xenobiotics and interpersonal differences in microbiome composition or remodeling. While mapping efforts have made significant progress in understanding interindividual variation in drug-microbiome interactions, similar approaches have not been applied to dietary xenobiotics.

To understand the scope and principles of interactions between the gut microbiome and dietary xenobiotics, we sought to systematically map the effects of chemically diverse dietary xenobiotics on bacterial growth and community composition and profile the capacity of diverse gut microbes and microbial communities to chemically modify these compounds. By integrating patterns highlighted in these maps, we identify mechanisms by which gut microbiome communities are remodeled by dietary xenobiotics and predict interindividual microbiome variability in the response to a given compound.

RESULTS

Generating maps of the growth impacts and metabolism of dietary xenobiotics

Many dietary xenobiotics ingested from foods such as fruits and vegetables (“parent” compounds) exist primarily as glycosides or esters, where a backbone is decorated with hydrophilic sugars (e.g., glucose, rhamnose, and rutinose) or acids (e.g., quinic acid and gallic acid). Other parent compounds exist only as undecorated backbones. To understand how microbial metabolism of these dietary xenobiotics contributes to differential responses to diet, we first explored the capacity of 29 human gut communities from unrelated, healthy donors (microbiome variation [MV] collection[35]) to metabolize 22 representative compounds (Figure 1A). This set of compounds included parent glycosides and esters and their undecorated derivatives, as well as undecorated parent compounds, from 13 different classes of dietary xenobiotics and included both compounds consumed in high doses from common foods (e.g., fruits and vegetables) as well as structurally related compounds consumed as dietary supplements or traditional medicines. Each compound was incubated with each human sample under anaerobic conditions in a culture medium that largely recapitulates microbiome composition in the human gut[36]; compound metabolism was measured after 48 h by liquid chromatography-mass spectrometry (LC-MS).

We observed a wide range of interindividual variability in the metabolism of different compounds by different communities, establishing three consistent patterns. Firstly, parent compounds with glycosidic linkages (e.g., polydatin and hesperidin) and ester bonds were readily cleaved by most or all communities, while their undecorated forms (e.g., resveratrol and hesperetin, respectively) were only metabolized by select communities (Figure 1A). Secondly, different human communities produced different metabolites from the same parent compound, including products of deglycosylation, ring-opening, double bond reduction, demethylation, and dehydroxylation (Figures S1A and S1B). Finally, polyphenols decorated with methoxyl groups were metabolized by fewer communities compared with undecorated polyphenols (e.g., naringenin vs. hesperetin; Figure 1A). The ability of individual members of the gut microbiome to metabolize methoxylated and non-methoxylated glycoside compounds *in vitro* is consistent with these community-wide measures (Figure S1C); for example, common members of the gut microbiome (*Bacteroides* and *Bifidobacteria* spp.) deglycosylate many of these compounds (Figure S1C), while less common taxa (e.g., acetogens) remove methoxyl groups from methoxylated polyphenols, likely through the Wood-Ljungdahl pathway[38] (Figure S1D).

These metabolic transformations of dietary xenobiotics by human gut communities and individual species included production or elimination of compounds reported to be antibacterial[39–41] (herein, toxicity refers to antibacterial activity). To determine whether microbial metabolism of dietary compounds alters xenobiotic toxicity, we first expanded our collection of dietary xenobiotics to include 161 compounds belonging to 37 structural classes (Figure 1B, Table S1). This expanded collection included parent compounds (glycoside, ester, or undecorated parents), undecorated derivatives (glycoside or ester hydrolysis products), and further downstream microbial metabolites (e.g., phenolic acids) (Figure S1A), allowing us to assess differences in toxicity between parent compounds and their microbial metabolites.

To determine relevant concentrations to test in our *in vitro* assays, we estimated human colonic concentrations of the dietary xenobiotics in our library after dietary consumption. Many polyphenols, especially glycoside or ester parent compounds, have limited bioavailability, and many of these glycosides are also resistant to human digestion (e.g., rhamnosides and rutinosides).[42–45] Up to 90% of a consumed dose can reach the colon, and so expected colon concentrations are significantly higher than expected serum concentrations.[46,47] We made estimates of small intestinal absorption based on ileostomy and fecal recovery data from over 50 literature sources, and for 93 compounds where data was available, calculated estimates of colon concentration using a previously described method[34] (see STAR Methods; Table S1; Figure S2A). We experimentally

(B) Compound classes represented in a library of 161 dietary xenobiotics.
(C) Growth of 26 gut commensal species in the presence of each dietary xenobiotic in the library (200 μM). Growth is normalized to the interquartile mean across all compounds for that species. Mean of two technical replicates is shown.
(D) Histogram of the number of species inhibited by each dietary xenobiotic. Compounds that inhibit two or more species are highlighted in orange and summarized in the pie chart.
See also Figure S1 and Tables S1 and S2.

validated our calculated estimates by directly measuring colonic concentrations of 11 compounds in germfree mice; for 9/11 compounds, measured concentrations were within 3-fold of calculated estimates (Figure S2B). For these 11 compounds, we also used *in silico* physiology-based pharmacokinetic modeling to predict pharmacokinetic properties, incorporating parameters for compound structure, absorption, and intestinal volume, and subsequently modeled their colonic concentrations in humans[48] (Figure S2C; Table S1); for 10/11 compounds, the modeled colonic concentrations matched our calculated estimates based on previous methods[34] within 3-fold. Having validated our calculated estimates, we found that two-thirds (64%) of compounds in our library were estimated to reach concentrations exceeding 200 μM in the colon (Figure S2D), and so used 200 μM as a physiologically relevant working concentration for further *in vitro* experiments.

Growth measurements of each of 26 bacterial species in the presence of each compound in the 161-compound dietary xenobiotic library revealed that over half of compounds (86/161) did not have a strong inhibitory effect (<50% growth) on any species, and only 14/161 (9%) inhibited growth of more than half of the tested species, suggesting that general antibacterial effects are uncommon at the tested xenobiotic concentration. However, we identified a subset of compounds (53/161; 32%) that reduce growth of at least 2 species by at least 50% at 200 μM (Table S1; Figures 1C and 1D). Concentrations of these compounds leading to 50% growth inhibition (IC_{50}) against a susceptible indicator species ranged from 50 to 250 μM; these IC_{50} values are lower than predicted colon concentrations for over half of the tested compounds (Table S1). Compound toxicity displayed phyla-level patterns: Proteobacteria were resistant to almost all compounds that inhibit most other phyla, while some compounds were preferentially toxic toward distinct phyla. Proteobacterial resistance is likely due to outer membrane impermeability and efflux because a hyperpermeable *Escherichia coli ΔbamB ΔtolC* mutant exhibited sensitivity to a large number of compounds (Figure 1C; Table S1).[49] Importantly, toxicity varies between parent compounds and their respective microbial metabolites; in multiple cases, glycosides are non-toxic while the corresponding non-glycosylated forms inhibit bacterial growth. In some cases, compounds representing further downstream metabolites of these toxic aglycones (reduced forms; altered carbon-carbon bonds) also do not inhibit bacterial growth.

Dietary xenobiotics remodel the composition of gut microbial communities

Given the widespread and variable capacity of dietary xenobiotics or their microbial metabolites to inhibit the growth of individual species, we next determined whether these compounds remodel the composition of microbial communities. To this end, we introduced 140 of the dietary xenobiotics from the 161-compound library (Table S1; 21 were excluded due to compound availability) to anaerobic incubations of four different microbial communities: three human communities from the set tested in Figure 1A (MV20, MV27, and MV29), and one 38-member defined community that included representatives of major human gut phyla along with species known to metabolize common dietary xenobiotics (Figure 2A; Table S2).

Using community composition measured by 16S sequencing, we assessed the β-diversity between samples (Figure 2B). Independent replicates of the same community treated with the same compound exhibited low β-diversity (95th percentile $\beta\text{-diversity}_{replicates} < 0.34$) (Figure 2C). To quantify the impact of dietary xenobiotics on community composition, we measured the β-diversity between a community grown with a dietary xenobiotic vs. its DMSO control ($\beta\text{-diversity}_{vs.\ DMSO}$). MV27 had higher overall $\beta\text{-diversity}_{vs.\ DMSO}$ scores than the other communities (Figure 2D), suggesting that it is more susceptible to disruption; this community also exhibited low α-diversity (Shannon entropy) and higher Clostridia relative abundance (Figures S2E and S2F). We used $\beta\text{-diversity}_{replicates}$ to estimate experimental and technical variation and identify compounds that significantly remodel communities (see STAR Methods) (Table S3; Figure 2D). In total, 25/140 compounds (19%) led to significant remodeling of at least one community (Figures 2D and S2G), and 10 of these 25 compounds disrupted all four communities ("pan-disruptive compounds") (Figure 2E). The changes induced by these pan-disruptive compounds were comparable to the differences between communities from different donors (inter-community β-diversity) (Figure 2E), suggesting that this extent of remodeling is relevant to microbiome function. The final density (OD_{600}) of these communities in the presence of the pan-disruptive compounds was also reduced compared with the DMSO controls, suggesting a reduction in absolute bacterial abundance (Figure S2H). Notably, pan-disruptive compounds were also toxic to gut commensals in pure culture (Figure 2E; Table S1). Indeed, when considering all compounds, average toxicity against single species in pure culture significantly correlated with $\beta\text{-diversity}_{vs.\ DMSO}$, demonstrating that compound toxicity is a major predictor of community remodeling under these conditions (Figure 2F).

We next assessed the change in relative abundance of individual taxa in a community in response to each dietary xenobiotic. Certain compounds, including pan-disruptive compounds, altered the relative abundances of the same bacterial classes across communities (Figure 3A; Table S4). Furthermore, shifts in community composition caused by these compounds were consistent with measured toxicity against individual species: the relative abundance of resistant taxa (e.g., Gammaproteobacteria) increased at the expense of susceptible taxa (Figure 3A). Of note, relative abundance measurements do not always reflect changes in absolute abundance when total bacterial load is altered, as we observed for highly toxic compounds (Figure S2H).

For most dietary xenobiotics, however, changes in taxa relative abundance were not shared between the four communities or predictable based on the compound's toxicity against related taxa in monoculture (Figure 3B). Furthermore, many compounds that caused only subtle changes in overall composition (low $\beta\text{-diversity}_{vs.\ DMSO}$) still showed significant changes in the relative abundance of multiple taxa (Tables S4 and S5). To more carefully dissect how an individual species' susceptibility to a dietary xenobiotic relates to its relative abundance in a community, we plotted the growth of a given strain treated with a given compound in monoculture (Figure 1C) against the relative abundance of the same strain in the 38-membered defined community treated with the same compound (Figure 3C; Table S5). In this

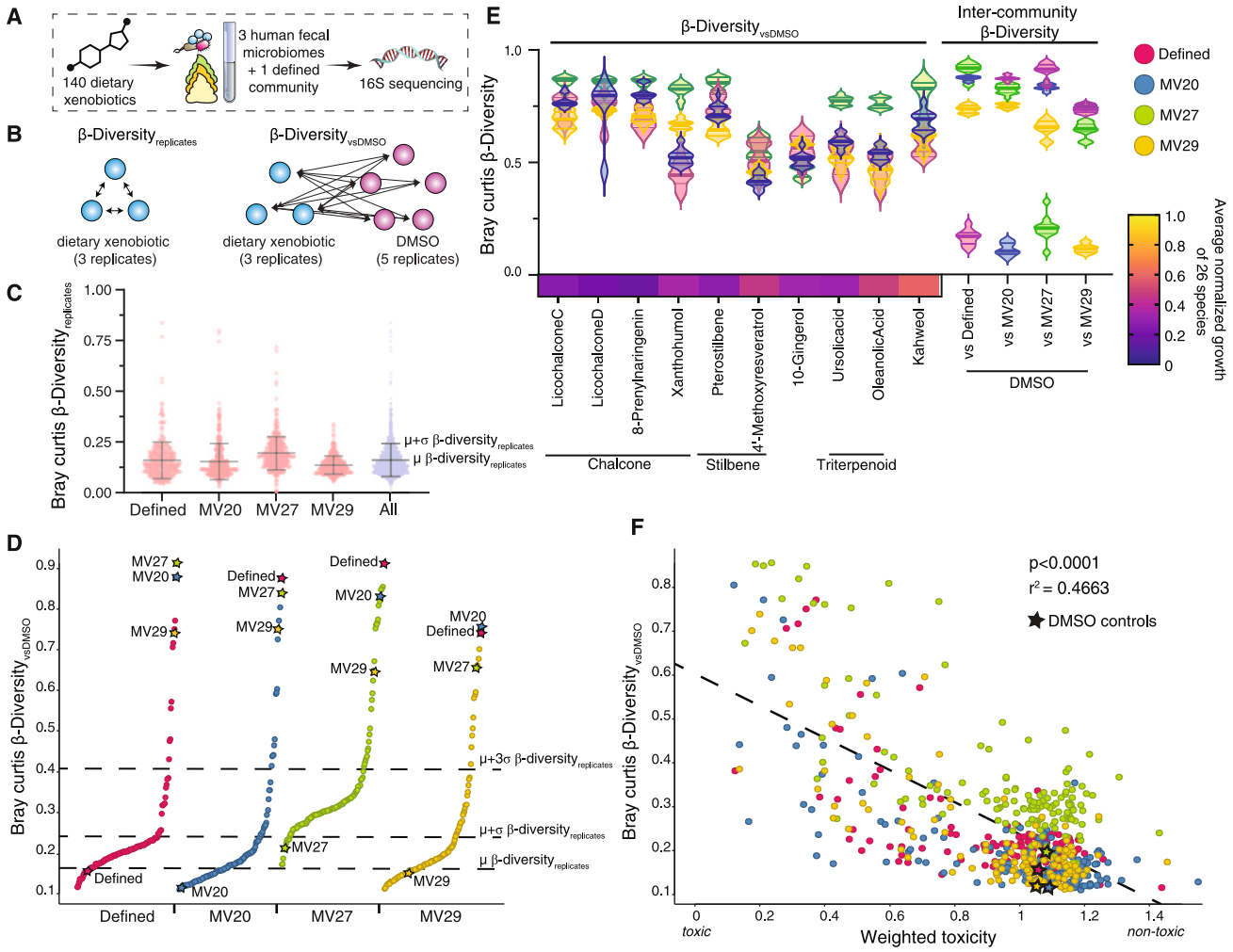

Figure 2. Mapping remodeling of human gut microbial communities by dietary xenobiotics

(A) Experimental setup for surveying the effects of 140 dietary xenobiotics on the composition of 4 gut microbiome communities.

(B) Schematic of β-diversity$_{replicates}$ and β-diversity$_{vs.\ DMSO}$ calculations. Each circle represents a single replicate.

(C) β-Diversity$_{replicates}$ across 140 dietary xenobiotics in each community. A line is drawn at the mean, and error bars represent standard deviation. Outlier replicates with high β-diversity$_{replicates}$ were removed from further analysis.

(D) Index plots show the β-diversity$_{vs.\ DMSO}$ of each community treated with each of the 140 dietary xenobiotics. Dashed lines represent cutoffs based on mean and standard deviation of β-diversity$_{replicates}$ in (B). See STAR Methods for details.

(E) Violin plot of ten dietary xenobiotics that remodel all four communities (β-diversity$_{vs.\ DMSO}$ > 0.41). Inter-community β-diversity is also shown for each pair of DMSO-treated communities. Toxicity is represented as a heatmap representing average normalized growth of 26 species in the presence of each compound (Figure 1C).

(F) Correlation between β-diversity$_{vs.\ DMSO}$ and weighted toxicity. Each point represents a given community treated with a given compound. r^2 value represents two-sided Pearson correlation. Weighted toxicity is a measure that captures growth inhibition of individual species in monoculture by a compound (as in Figure 1C), weighted according to the relative abundance of related taxa in each community (Figure S2F). In (D) and (F), comparisons to communities from unrelated human donors are indicated by stars. In (D)–(F), mean of β-diversity$_{vs.\ DMSO}$ is plotted (5 DMSO replicates × 3 dietary xenobiotic replicates = 15).

See also Figure S2 and Table S3.

plot, most points fall within a normal distribution along each axis, since most compounds are non-toxic in monoculture and also have no effect on community composition. Additionally, some compounds that are toxic in monoculture lead to predictable depletion of susceptible taxa. Points falling outside of these expected regions represent emergent interactions: cross-sensitization occurs when a compound reduces the relative abundance of a species in a community but has little or no activity against that species in monoculture, whereas cross-protection occurs when a compound exhibits significant toxicity against a species in monoculture but does not reduce the relative abundance of that species in the community context.

To probe how compound metabolism is related to emergent interactions, we used LC-MS to measure the levels of each compound after incubation with the 38-member community. Compounds that predictably depleted taxa in the community

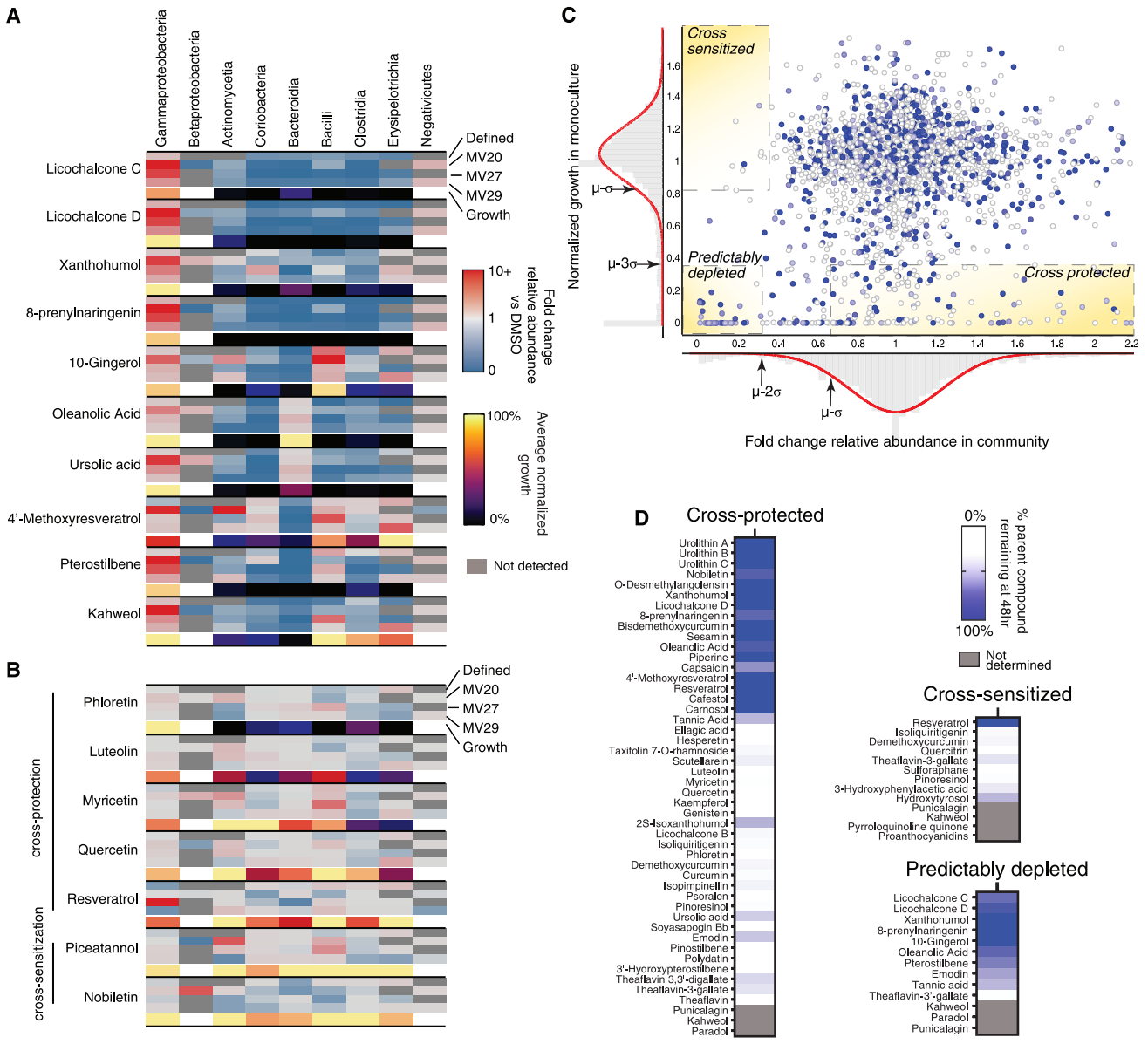

Figure 3. Predicted and emergent interactions between dietary xenobiotics and community composition

(A and B) For each dietary xenobiotic, the fold change in relative abundance of bacterial classes within each community is compared with the average toxicity of the compound toward representative species in this class. (A) For ten compounds that remodel all four tested communities, the taxa that change in relative abundance are predicted by the spectrum of toxicity of the compound toward each bacterial class. (B) Examples of emergent interactions in which toxic effects of a compound on individual species in monoculture do not predict community remodeling.

(C and D) (C) Response of 26 species in a 38-member defined community and in monoculture to the presence of each of 140 dietary xenobiotics. Each point represents the normalized growth of a species treated with the given compound in monoculture (from Figure 1C) vs. its fold change relative abundance (vs. DMSO) in the 38-member community. Histograms along the x and y axes demonstrate Gaussian distributions that define cutoffs for predicted or emergent interactions, as indicated. Dietary xenobiotics falling into each category are listed in (D). Metabolism of the dietary xenobiotic by the defined community, normalized to a sterile media control, is represented by color shading in (C) and (D). For all panels, mean of triplicate incubations is shown.

See also Tables S4 and S5.

based on toxicity in monoculture, including 8 of the 10 pan-disruptive compounds, were generally not metabolized by the 38-member community (Figure 3D). By contrast, most compounds involved in cross-protection or cross-sensitization interactions were substantially metabolized by the 38-member community, with less than 25% of the parent compound remaining (Figure 3D). These results suggest that metabolism of dietary xenobiotics may be related to the observed emergent interactions. Notably, there are exceptions to this trend, and so alternate mechanisms not related to metabolism could also occur.

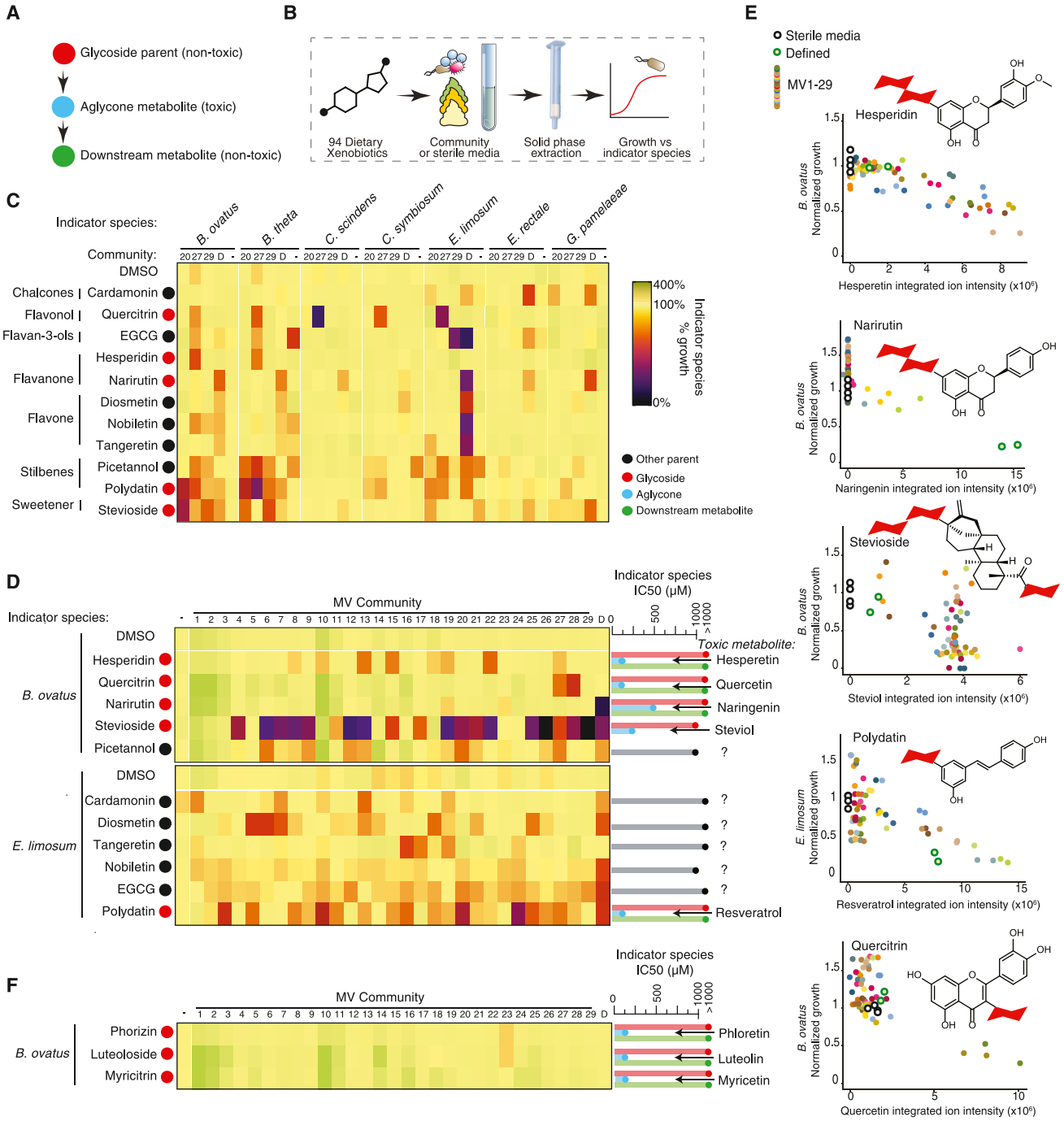

Figure 4. Toxification and detoxification of dietary xenobiotics by the gut microbiome

(A) Model for microbiome-mediated toxification and detoxification of dietary xenobiotics.

(B) Experimental workflow for generation and characterization of extracts from microbial communities incubated with dietary xenobiotics.

(C and D) Normalized growth of indicator species (vs. DMSO) with extracts prepared from communities labeled along the top and dietary xenobiotics labeled along the left. (C) For 11 of 94 dietary xenobiotics tested, extracts prepared from incubation of the compound with at least one community inhibited the growth of at least one indicator species (<40% growth). Extracts of compounds alone (columns labeled with "-") and communities alone (DMSO row) did not inhibit growth of these indicator species, apart from examples of inhibition of *B. thetaiotaomicron* and *E. limosum*. (D) Toxification of the 11 compounds in (C) by 29 human fecal microbial communities. Bar graphs along the right indicate the IC_{50} of these dietary xenobiotics and their metabolites, colored according to the scheme in (C).

(E) Relationship between normalized growth of an indicator species and the detection of toxic aglycones. Each point represents an individual extract prepared from a different MV community. The mean growth of technical duplicates is plotted on the y axis.

(legend continued on next page)

Together, these results illustrate the intuitive principle that compounds inhibiting the growth of bacteria lead to community remodeling based on their spectrum of toxicity, as exemplified by the ten pan-disruptive compounds. In many cases, however, the impact of a dietary xenobiotic on a given community is not so readily predicted, revealing emergent interactions.

Dietary xenobiotics are variably toxified or detoxified by human communities

We hypothesized that variable microbial metabolism of dietary xenobiotics could produce emergent properties such as cross-sensitization and cross-protection by altering compound toxicity (Figure 4A). To create a detailed map of how the toxicity of dietary xenobiotics is modified by community metabolism, we selected 94 of the dietary xenobiotics from the 161-compound library (Table S1; the excluded compounds were pan-disruptive, less common in foods, or cost prohibitive), incubated each of these compounds with the four microbial communities (MV20, MV27, MV29, and the 38-member defined community) used above, generated small-molecule extracts from each incubation, and measured the capacity of these extracts to inhibit the growth of seven representative gut commensals (Figure 4B). Extracts prepared from each of these four communities in the absence of added dietary xenobiotics were non-toxic to the seven indicator species (Figure 4C).

For 11/94 compounds ("toxified compounds"), growth of at least one indicator species was inhibited by an extract prepared after incubation with at least one community, indicating the potential production of a toxic metabolite (Figures 4C and S3A; in each case, the parent compound was non-toxic). Several compounds in this set (e.g., quercitrin, polydatin, piceatannol, and nobiletin) also displayed community-specific remodeling activity in a manner that was not predicted by their impact on growth of single species in pure culture, suggestive of community-specific emergent interactions (Figure 3B). When these 11 compounds were each incubated with the 29 human microbiome communities from the MV collection (Figure 1A), extracts from these incubations produced community- and compound-specific capacity to inhibit growth of indicator species (Figure 4D).

Five of these toxified compounds (hesperidin, narirutin, quercitrin, stevioside, and polydatin) are glycosides whose aglycone forms demonstrate toxicity but whose downstream metabolites are non-toxic (Figures 4A and S3B). These glycosides were deglycosylated to toxic aglycones by almost all 29 human communities but then variably metabolized to non-toxic downstream metabolites by some communities and not others (Figure S3C). The correlation between aglycone abundance in extracts prepared from compounds incubated with the 29 communities and growth inhibition of the indicator species suggests these aglycones are responsible for the observed toxicity (Figure 4E). Toxification of the glycoside polydatin by community MV20 provides an example: we incubated polydatin with MV20, used activity-guided purification to isolate the toxic factor produced in these incubations, and identified this factor as the polydatin aglycone resveratrol using LC-MS (Figure S3D). It is possible that some compounds additionally induce a community to produce unrelated metabolites that either increase or decrease the growth of indicator species. For example, this could explain the observation that extracts prepared from incubations of different communities with stevioside have varying impacts on *B. ovatus* growth, despite similar levels of steviol in these extracts (Figure 4E).

For some glycosylated parent compounds whose aglycone form is toxic, extracts prepared from incubation of the parent compounds with MV20, MV27, MV29, or the 38-member defined community did not inhibit growth of the indicator species despite disappearance of the parent compounds. Incubating three of these glycosides (phlorizin, luteoloside, and myricitrin) with the complete set of 29 human communities did not reveal toxification in any instance, and LC-MS revealed that predicted toxic aglycones were uniformly metabolized into non-toxic downstream metabolites (Figures 4F, S3C, and S3E). Consistently, direct addition of these compounds to the tested communities did not result in community remodeling, despite the toxicity of their aglycone forms (Figure 3B). In contrast to these universally detoxified compounds, methoxylated compounds (e.g., hesperetin, diosmetin, and tangeretin) are transformed to downstream metabolites by a smaller subset of communities and thus exhibit a greater variability in their toxic effects (Figure 4D). Therefore, for these glycosides, the extent of metabolism of the toxic aglycone determines whether a toxic or non-toxic metabolite accumulates.

For the remaining six toxified compounds that are not glycosides (diosmetin, piceatannol, cardamonin, nobiletin, tangeretin, and epigallocatechin gallate [EGCG]) (Figure 4C), the identity of the metabolite(s) responsible for toxicity is not clear. In some cases, reported metabolites of these dietary xenobiotics were produced to variable levels by the different human communities but did not correlate with growth inhibition of the indicator species, suggesting that they are not responsible for toxicity (Figure S3F). It is possible that toxicity in these extracts results from other transformation products of the dietary xenobiotic or from unrelated metabolites induced in the community. Since we observed weak growth inhibition by some compounds at very high concentrations (i.e., nobiletin and piceatannol; Figure 4D), it is also possible that toxicity of the dietary xenobiotic itself is enhanced by other components of the extracts. Together, these results provide guiding principles that explain how many dietary xenobiotics are variably metabolized by gut microbial communities and are toxified or detoxified as a result, although additional processes likely also contribute to these interactions.

Dietary xenobiotic metabolism predicts community remodeling *in vitro*

By combining insights into dietary xenobiotic toxicity, remodeling capacity, and metabolism, we envisioned mechanisms by

(F) Examples of compounds where incubation with 29 human communities never results in toxification, since toxic aglycone forms are invariably detoxified through microbial metabolism, as shown in Figure S3B. For normalized growth in (C), (D), and (F), mean of two independent extract preparations followed by two independent growth measurements (total of $n = 4$) is shown; "D" indicates defined community and "-" indicates sterile media.
See also Figure S3.

which dietary xenobiotics interact with the gut microbiome to explain emergent properties (cross-sensitization/cross-protection) and variability in the effects of a compound on different communities. We hypothesized that microbial metabolism of non-toxic dietary xenobiotics could produce toxic metabolites that deplete susceptible species, thus resulting in cross-sensitization. Additionally, microbial metabolism could detoxify otherwise toxic dietary xenobiotics or their aglycones, resulting in cross-protection of susceptible species.

We selected three dietary xenobiotics (polydatin, hesperidin, and stevioside) to test these hypothesized mechanisms (Figure 5). We chose these compounds because (1) they were variably metabolized by human communities both *in vitro* and in gnotobiotic mice colonized with human communities (Figures 1A and S4A); (2) they were toxified by community metabolism through production of the cognate aglycone (Figures 4D and 4E); (3) they are commonly consumed (polydatin in grapes or as a supplemental tablet, hesperidin in citrus fruits, and stevioside as a non-caloric sweetener; Table S1) and are implicated in human health[50–52]; and (4) the doses that are commonly consumed produce colonic concentrations relevant for community remodeling (200 μM). For example, the minimum inhibitory concentration (MIC) of the aglycone forms of polydatin, hesperidin, and stevioside against susceptible taxa are ∼125–250 μM (Figure S4B), which are exceeded in the colonic contents of mice gavaged with relevant doses (Figure S4A).

To mechanistically test these hypothesized mechanisms for community remodeling, we identified species capable of metabolizing polydatin, hesperidin, or stevioside (Figure S4C), constructed 8–10 membered defined communities variably containing these species, and measured community remodeling upon introduction of each parent glycoside, aglycone, and downstream metabolite. We first examined polydatin, a 3-glucosylated stilbene (IC_{50} > 1,000 μM) that is deglycosylated to form the aglycone resveratrol ($IC_{50} \geq$ 125 μM); subsequent reduction produces dihydroresveratrol (IC_{50} > 1,000 μM) (Figure 5A). While many species are capable of deglycosylating polydatin to resveratrol (Figure S1C), only two species in our collection (*Eggerthella lenta* DSM 2243 and *Adlercreutzia equolifaciens* DSM 19450; both phylum Actinobacteria, class Coriobacteriia) reduce resveratrol to dihydroresveratrol (Figure S4C), consistent with previous reports.[53] In a 9-membered community lacking *E. lenta* or *A. equolifaciens*, addition of polydatin resulted in cross-sensitization: resveratrol accumulated (Figure S4D), while the relative abundance of *Bacteroides thetaiotaomicron* was significantly reduced (Figure 5B), consistent with its sensitivity to resveratrol but not polydatin (Figure S4B). Direct addition of resveratrol to this community modulated community composition in a similar manner (Figure 5B). Adding *E. lenta* to the community resulted in cross-protection: when polydatin was administered, dihydroresveratrol accumulated instead of resveratrol, and *B. thetaiotaomicron* remained stable in the community (Figures 5B and S4D).

As a second example, we examined hesperidin, a 7-O-rutinoside with an IC_{50} > 1,000 μM. Hesperidin is deglycosylated to form the aglycone hesperetin, a 4′-methoxylated flavanone with $IC_{50} \geq$ 125 μM (Figure 5C). Hesperitin is subsequently metabolized to phenolic acids (e.g., 3-(4-methoxy-3-hydroxyphenyl) propionic acid (MHPPA); IC_{50} > 1,000 μM); we also identified species capable of demethylating hesperetin to eriodictyol (Figure S4C). Of the 30 species tested, only *Ruminococcus gnavus* ATCC 29149 metabolized hesperidin to hesperetin (Figure S1C); consistent with previous reports,[54,55] *E. ramulus* DSM 16296 transformed hesperidin or hesperetin to MHPPA (Figure S4C). In a 9-membered community lacking *R. gnavus* or *E. ramulus*, the glycoside hesperidin was not metabolized (Figure S4E) and had minor effects on community composition, while the aglycone hesperetin caused depletion of *B. thetaiotaomicron* and *B. ovatus* (both relative and absolute abundance, Figures 5D and S4F). Addition of *R. gnavus* or *E. ramulus* to this community resulted in cross-sensitization to hesperidin or cross-protection from hesperetin, respectively, consistent with metabolite accumulation through this pathway in each community (Figures 5D, S4E, and S4F). The relative abundance of *E. ramulus* also expanded in the presence of these compounds, consistent with its utilization of hesperidin/hesperetin and with its expansion in human subjects consuming a flavonoid-rich diet.[56]

As a third example, we examined stevioside (IC_{50} > 1,000 μM), composed of three glucose moieties decorating a steviol aglycone core ($IC_{50} \geq$ 250 μM) (Figure 5E). We identified species capable of cleaving each glycosidic linkage in stevioside, ultimately producing steviol, which is not further degraded (Figures 5E and S4C). *Blautia producta* DSM 3507 was capable of fully metabolizing stevioside to steviol, and its inclusion in a defined community resulted in cross-sensitization of *B. thetaiotaomicron* to stevioside (Figures 5F and S4G). Direct addition of the aglycone steviol similarly depleted the relative abundance of *B. thetaiotaomicron*, which was independent of *B. producta* as expected (Figure 5F).

It was notable that each aglycone, whether added directly or accumulated due to metabolic transformations, primarily depleted *B. thetaiotaomicron* from these 9-member communities despite the presence of other susceptible species. To test whether this was community dependent, we assembled eight other defined communities with different *Bacteroides* spp. and measured community disruption by hesperetin and resveratrol (Figure S4H). In most cases, *Bacteroides* spp. were preferentially depleted over other susceptible genera, but the species most significantly depleted did not correlate with growth rate or with IC_{50} in monoculture (Figure S4H). This finding suggests that as observed for other community perturbations,[57,58] context-dependent interactions such as metabolic cross-feeding and exploitative or interference competition[59,60] likely play a role in shaping community response to disruption.

Building on these results from 9 to 12 membered synthetic bacterial communities, we next tested whether cross-sensitization and cross-protection through dietary xenobiotic metabolism could also predict remodeling of complex, unfractionated human gut microbial communities. Our previous data measuring the impact of hesperidin on three communities (MV20, MV27, and MV29) supported the possibility that metabolism of hesperidin to hesperetin predicts remodeling, as assessed by $\beta\text{-diversity}_{\text{vs. DMSO}}$ (Figure S5A; Table S3). These communities exhibited similar metabolism of stevioside and polydatin, precluding efforts to relate metabolism of these compounds with remodeling. Thus, we extended our survey of human communities, focusing on polydatin. To this end, we treated the

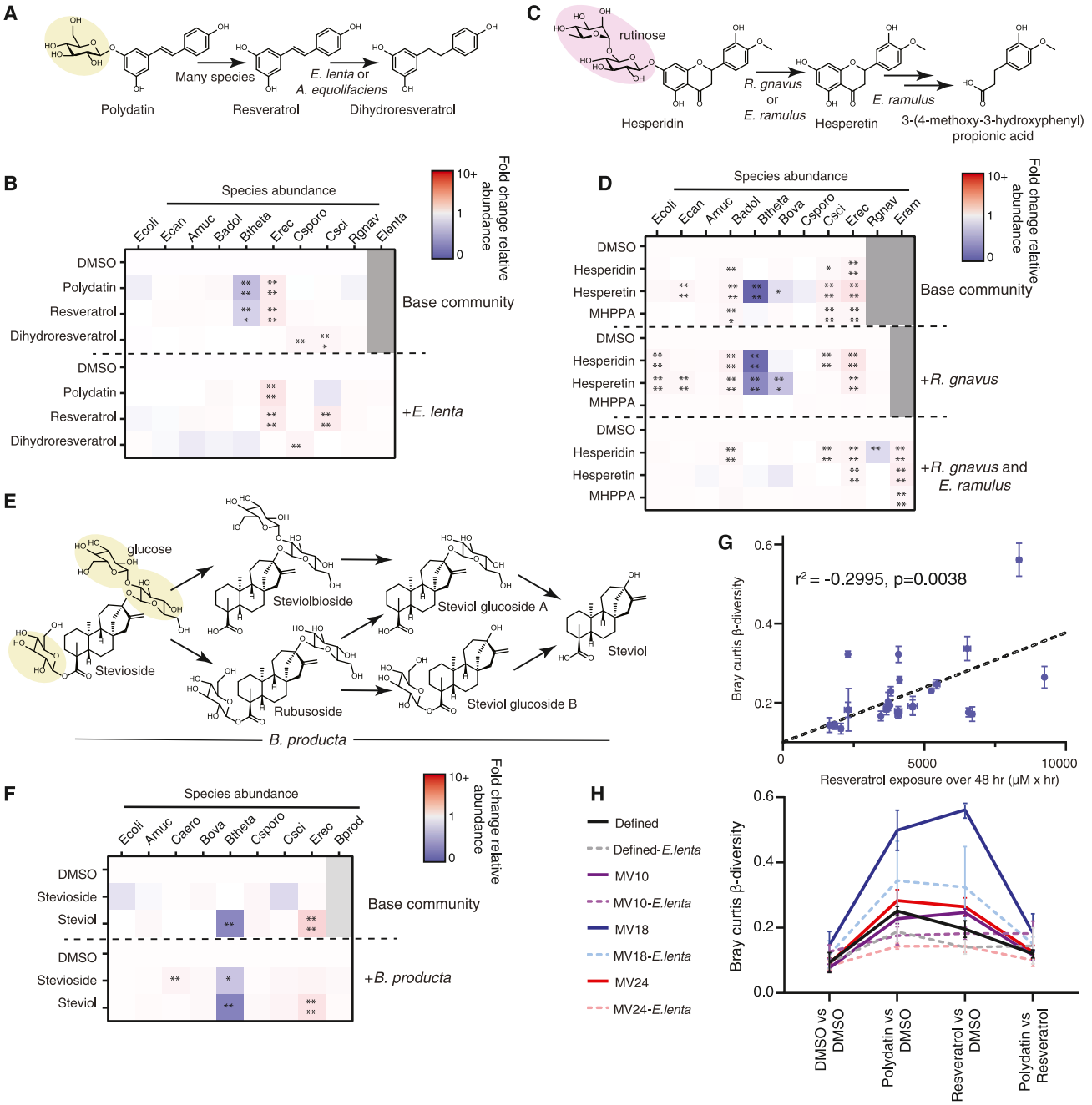

Figure 5. Microbial metabolism links community remodeling with dietary xenobiotic toxicity

(A–F) (A and B) Polydatin, (C and D) hesperidin, and (E and F) stevioside remodel 8–10 membered defined communities *in vitro*. (A, C, and E) Metabolic pathways and metabolizing species. (B, D, and F) Fold change relative abundance vs. DMSO of each species (columns) after introduction of these xenobiotics or their metabolites (rows). Full species names are provided in Table S2. Mean of four replicate incubations is shown, and statistically significant differences compared with the DMSO control are indicated (*$p < 0.05$, **$p < 0.01$, ***$p < 0.001$, ****$p < 0.0001$; two-way ANOVA with Tukey's post hoc analysis).

(G) Correlation between β-diversity$_{vs.\ DMSO}$ and resveratrol exposure over 48 h for 25 complex human fecal communities incubated *in vitro* with 200 μM resveratrol. r^2 value indicates Pearson correlation.

(H) Addition of *E. lenta* modulates community remodeling in response to polydatin or resveratrol. (G) Mean and standard deviation of three replicate incubations were measured for ion abundance (resveratrol exposure). (G and H) Mean and standard deviation of β-diversity between two compounds with three replicates each (DMSO vs. DMSO: $n = 3$; polydatin/resveratrol vs. DMSO or polydatin vs. resveratrol: $n = 3 \times 3 = 9$) are shown.

See also Figures S4 and S5.

human gut communities from the MV collection (Figure 1A) with polydatin, resveratrol, or DMSO *in vitro* and measured compound metabolism and community composition (Figures S5B and S5C). In communities incubated with polydatin, exposure to resveratrol was significantly correlated to β-diversity$_{vs.\ DMSO}$ (Figure 5G). Polydatin-induced compositional changes were similar to those resulting from direct resveratrol addition, as indicated by low β-diversity and significantly correlated changes in bacterial taxa relative abundance between these treatments (Figures 5G, S5E, and S5F). Further, addition of the cross-protective strain *E. lenta* to communities characterized by slow resveratrol detoxification or to a non-metabolizing 38-membered defined community reduced resveratrol exposure (Figure S5D) and community disruption by both polydatin and resveratrol (Figure 5H). The 38-member defined community demonstrated predictable emergent interactions: for example, *B. ovatus* was cross-sensitized to polydatin in the absence of *E. lenta* and cross-protected from resveratrol in the presence of *E. lenta* (Figure S5G). We also observed cross-protective interactions in the absence of *E. lenta*, suggesting additional mechanisms outside of detoxification that remain to be elucidated. Together, these results provide *in vitro* evidence that cross-sensitization and cross-protection are one major mechanism by which dietary xenobiotics remodel microbial communities.

Identification of a resveratrol reductase in Coriobacteriia

We sought to understand the genes and enzymes involved in dietary xenobiotic toxification and/or detoxification. Like many metabolic transformations of dietary xenobiotics by the gut microbiome, the specific enzymes responsible for resveratrol metabolism are unknown. We found that cell-free lysates produced from *E. lenta* grown in the presence of resveratrol, but not in its absence, could reduce resveratrol (Figure 6A), suggesting that the responsible gene may be transcriptionally regulated. Therefore, we performed RNA sequencing (RNA-seq) of *E. lenta* to identify genes upregulated by resveratrol. Only 26 genes were significantly upregulated, including 2 operons (Figure 6B; Table S6). Two genes were upregulated over 100-fold and had annotated functions likely to be involved in electron transfer: *Elen_288*, annotated as a fumarate reductase, and *Elen_1284*, annotated as a flavodoxin family protein.

We used CRISPR[61] to delete either *Elen_288* or the three-gene operon including *Elen_1284* (Figures S6A and S6B) from *E. lenta*. Deleting *Elen_288*, but not *Elen_1283-5*, abolished resveratrol reduction in *E. lenta* (Figure 6C). Heterologous expression of Elen_288 in a non-metabolizing Coriobacteriia, *Gordonibacter urolithinfaciens*, conferred resveratrol reductase activity. Thus, Elen_288 is necessary and sufficient for resveratrol reduction (Figure 6C). It is possible that Elen_1284 is not involved in resveratrol reduction or that its function is redundant with other proteins and thus dispensable.

Elen_288 is a predicted TAT-secreted flavinylated lipoprotein with previously characterized homologs in *Listeria monocytogenes* and *Enterococcus rivorum* (Figure S6C).[62] This family of proteins is involved in extracellular electron transport for the reduction of terminal electron acceptors supporting anaerobic respiration (Figure S6C). Previously characterized Elen_288 homologs reduce fumarate or urocanate, which are structurally distinct from resveratrol on both sides of the targeted double bond.[62] BLASTP analysis of RefSeq identified Elen_288 homologs in Coriobacteriia but not other bacterial classes. Consistent with our phenotypic evidence (Figure 6C), the metabolizing species *A. equolifaciens* DSM 19450 encodes a close homolog (Aequ_2118, with 76.3% amino acid identity), while non-metabolizing species *Gordonibacter pamelaeae*, *G. urolithinfaciens*, and *Slackia isoflavoniconvertens* encode only distant homologs (<42% amino acid identity). Using this data to support 70% as an amino acid identity cutoff that predicts resveratrol reductase activity, we mapped the presence of Elen_288 homologs in 96 Coriobacteriial genomes (Figure 6D). We found that the gene is largely restricted to *Eggerthella*, *Adlercreutzia*, and *Raoultibacter* spp. and is highly conserved in *E. lenta* strains.

Having identified the species and genes responsible for resveratrol reduction, we asked whether its abundance in microbial communities could predict the metabolism of resveratrol. Using primers targeting conserved regions of resveratrol reductase homologs in *Eggerthella*, *Adlercreutzia*, or *Raoultibacter*, we measured gene abundance in our MV human community collection after *in vitro* culturing. *E. lenta* species abundance was strongly correlated with resveratrol reductase gene abundance, consistent with its high conservation in this species (Figure 6E). Furthermore, *Eggerthella* resveratrol reductase gene abundance was significantly correlated with the rate of resveratrol reduction by the communities (Figure 6F). *Adlercreutzia* and *Raoultibacter* resveratrol reductase gene abundance was below the limit of detection, consistent with low abundance of these species under these *in vitro* conditions.

We next tested whether Elen_288 determines the ability of *E. lenta* to protect a community from disruption by polydatin or resveratrol. Indeed, while wild-type *E. lenta* can protect a 9-member community from disruption by polydatin or resveratrol (Figure 5B), the isogenic *E. lenta* Δ*Elen_288* strain fails to protect *B. thetaiotaomicron* from depletion despite maintaining equivalent relative abundance as the wild-type *E. lenta* strain (Figures S6D and S6E). These results demonstrate that by understanding mechanisms of dietary xenobiotic community remodeling, the response of a community to a given compound can potentially be predicted and altered based on a single gene.

Dietary xenobiotic metabolism predicts community remodeling *in vivo*

Finally, we tested whether our model of dietary xenobiotic community remodeling extends to the mammalian gut environment. Focusing on polydatin, we first colonized germfree mice with the 9-membered multi-phylum community with or without *E. lenta*, as previously characterized *in vitro* (Figure 5B). We monitored microbiome composition in fecal samples during a control window (PBS gavage) and treatment window (polydatin gavage) (Figures 7A and S7A). During the treatment window, fecal resveratrol levels approximated 200 μM, consistent with predicted colonic concentrations in humans (Table S1; Figure 7B). Consistent with resveratrol reduction by *E. lenta* in the gut, inclusion of *E. lenta* in the community significantly altered exposure to polydatin and its metabolites both locally and systemically: fecal resveratrol levels were significantly reduced,

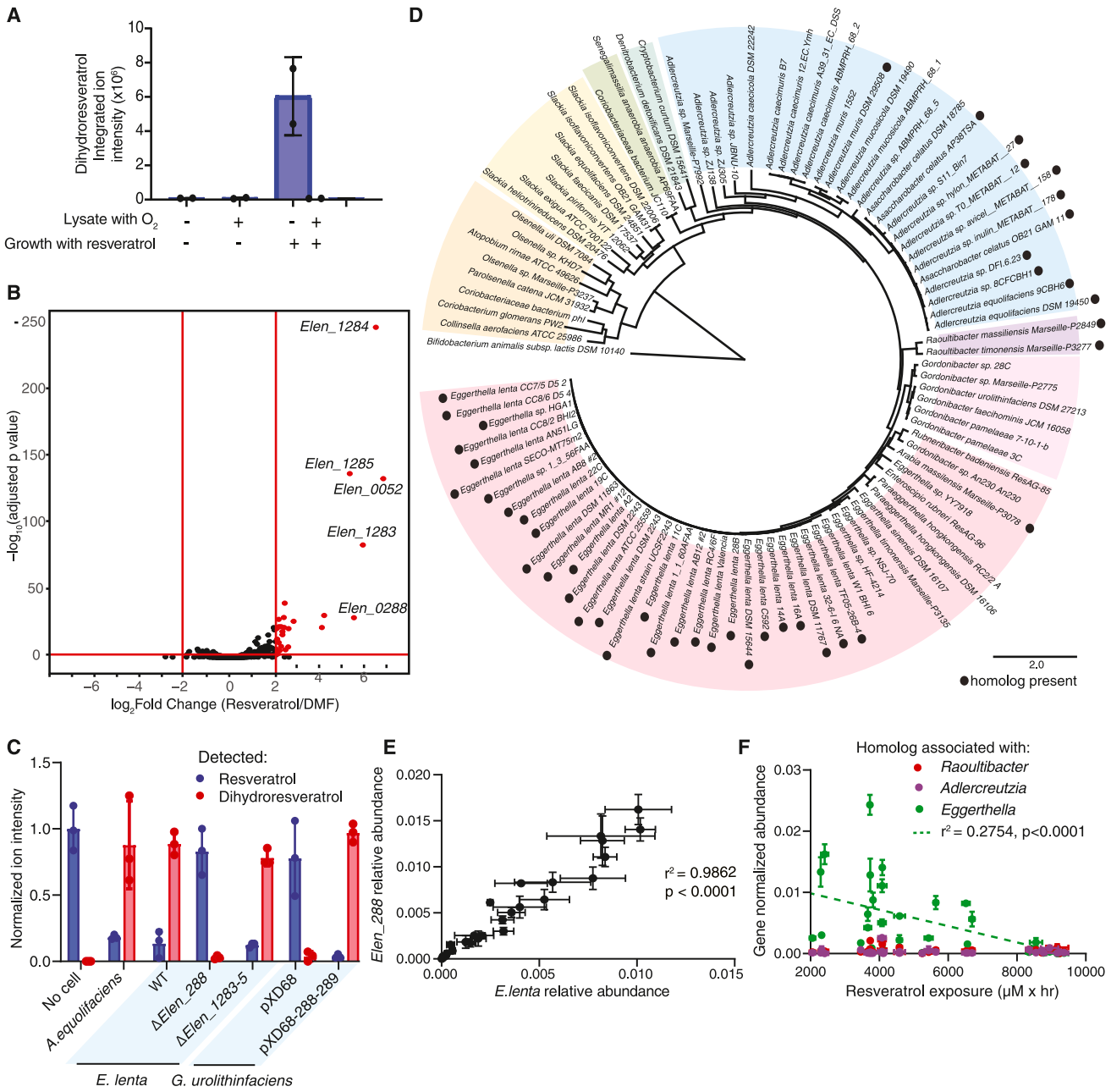

Figure 6. Identification of a resveratrol reductase in Coriobacteriia

(A) Cell-free lysates generated from *E. lenta* grown in the presence or absence of 100 μM resveratrol were tested for their ability to reduce resveratrol to dihydroresveratrol. Incubations of cell-free lysates in aerobic or anaerobic conditions are indicated. Mean and standard deviation of duplicates are shown.

(B) A volcano plot shows differential transcript abundance, determined by RNA-seq, for *E. lenta* grown in the presence of 100 μM resveratrol or vehicle (dimethylformamide [DMF]).

(C) The ability of various species or strains to metabolize resveratrol to dihydroresveratrol was measured by *in vitro* incubation and LC-MS. Ion intensity is normalized to the sterile medium control. *G. urolithinfaciens* includes an empty vector control (pXD68) or a vector carrying *Elen_288-289* (pXD68-288-289); *Elen_289* is a putative transcriptional regulator that activates the expression of *Elen_288* in response to resveratrol.

(D) Phylogenetic tree of 96 Coriobacteriial strains with the presence of *Elen_288* homologs indicated by black dots.

(E) Correlation between the abundance of *Elen_288* and the abundance of *E. lenta* in 29 MV communities grown *in vitro*, as determined by qPCR using gene- and species-specific primers.

(F) Correlation between the abundance of resveratrol reductase homologs associated with different genera (*Eggerthella*, *Adlercreutzia*, and *Raoultibacter*) and the rate of resveratrol metabolism (as in Figure 5G) by 29 MV communities incubated *in vitro*. For (E) and (F), Pearson correlation is shown. For (C), (E), and (F), mean and standard deviation of three replicate incubations are shown.

See also Figure S6 and Table S6.

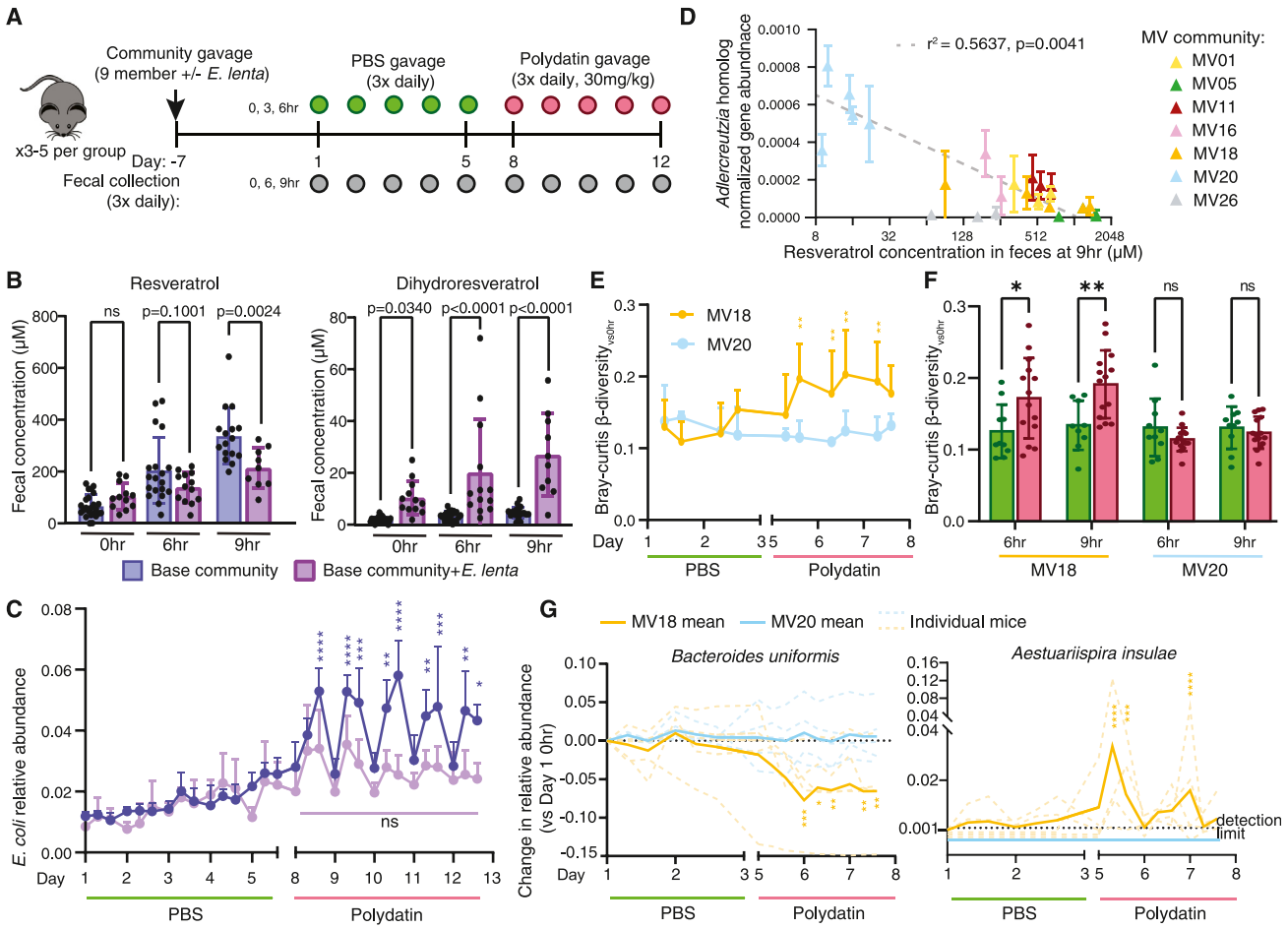

Figure 7. Metabolism of resveratrol by gut microbes dictates community remodeling by polydatin *in vivo*

(A–C) A defined community is remodeled by polydatin in gnotobiotic mice. (A) Experimental design using defined communities as in Figure 5B. (B) The concentration of resveratrol and dihydroresveratrol in feces collected at 0, 6, or 9 h time points daily during polydatin treatment. Points represent 5 days of treatment with 5 mice (base community: $n = 25$) or 3 mice (base community + *E. lenta*: $n = 15$). (C) Relative abundance of *E. coli* in feces during PBS or polydatin treatment. Significance is tested compared with day 1 at 0 h for the base community ($n = 5$ mice) or base community + *E. lenta* ($n = 3$ mice).

(D) Relationship between *Adlercreutzia* resveratrol reductase gene abundance and resveratrol metabolism in ex-germfree mice colonized with fecal microbial communities from 7 human donors. Each point represents an individual mouse with gene abundance measured across 4 days. Pearson correlation is shown.

(E–G) Impact of polydatin on the microbiomes of ex-germfree mice colonized with either MV18 or MV20. (E and F) $\beta\text{-diversity}_{\text{vs. 0 h}}$ is calculated between the 0 and 6 h time points, or 0 and 9 h time points on the same day. In (E), significant differences between MV18 $\beta\text{-diversity}_{\text{vs. 0 h}}$ and MV20 $\beta\text{-diversity}_{\text{vs. 0 h}}$ at each time point are indicated ($n = 5$ mice/group). In (F), significant differences between PBS and polydatin treatment periods are indicated. Points represent 5 mice across 2 days of PBS treatment ($n = 10$; green) or 5 mice across 3 days of polydatin treatment ($n = 15$; pink). (G) Change in relative abundance of *B. uniformis* or *A. insulae* during PBS or polydatin treatment. Significant changes in relative abundance were determined by comparison to day 1 at 0 h ($n = 5$ mice/group). For all panels, mean and standard deviation are shown. Significance is tested using one-way (B and C) or two-way ANOVA (E–G) with Tukey's (B), Bonferroni's (E and F), or Dunnett's (C and G) post hoc analysis. $^{*}p < 0.05$, $^{**}p < 0.01$, $^{***}p < 0.002$, $^{****}p < 0.0001$.

See also Figure S7 and Table S7.

while fecal dihydroresveratrol was significantly elevated (Figure 7B). Further, inclusion of *E. lenta* in the community significantly reduced serum levels of resveratrol and its host-mediated (glucuronidated and sulfated) metabolites and significantly elevated serum levels of host-mediated dihydroresveratrol metabolites (Figure S7B). While composition of communities with and without *E. lenta* was stable during the control window, the community lacking *E. lenta* exhibited daily disruption during the polydatin treatment window. During disruption, *E. coli* (which is resistant to growth inhibition by resveratrol, Figure S4B) expanded 3- to 4-fold in relative and absolute abundance (measured by colony-forming unit [CFU]) daily upon polydatin treatment and returned to baseline levels by the next morning when resveratrol had passed through the gut (Figures 7C and S7A). Consistent with the capacity of *E. lenta* to detoxify resveratrol to dihydroresveratrol, addition of *E. lenta* protected the community (including *E. coli*) from disruption by polydatin (Figure 7C and S7C).

We noted that while polydatin disrupts the composition of this 9-membered community in an *E. lenta*-dependent manner both

in vitro and *in vivo*, the specific species affected differ: in the absence of *E. lenta*, *Bacteroides* spp. are depleted *in vitro*, while *E. coli* expands *in vivo*. Cell density likely contributes to these differences: incubating fecal material from mice carrying the 9-membered community (lacking *E. lenta*) with resveratrol *ex vivo* with minimal dilution recapitulated the pattern of *E. coli* expansion observed *in vivo*, while further dilution of the same fecal samples resulted in depletion of *B. thetaiotaomicron* and other susceptible species upon resveratrol treatment (Figure S7D).

Next, we investigated resveratrol metabolism in complex, unfractionated gut microbial communities *in vivo*. To this end, we colonized groups of germfree mice with fecal microbiomes from 7 unrelated human donors, administered polydatin, and quantified the levels of polydatin and its metabolites in fecal samples. We observed fecal resveratrol concentrations that spanned over 160-fold (9–1,500 μM) across mice colonized with different human communities (Figure 7D), highlighting the wide, microbiome-dependent variability in dietary xenobiotic metabolite concentrations in response to consumption of the same amount of the parent compound. In this *in vivo* setting, the abundance of *Eggerthella* and *Raoultibacter* resveratrol reductase homologs does not correlate with resveratrol levels after polydatin treatment (Figures S7E and S7F), while the abundance of the *Adlercreutzia* resveratrol reductase homolog *Aequ_2118* in these communities robustly predicts the extent of polydatin metabolism to resveratrol in these animals (Figure 7D). The poor growth of *Adlercreutzia* in the *in vitro* conditions tested, combined with possible differences in gene regulation, may contribute to this discrepancy. These observations suggest that molecular markers such as gene abundance can be an important tool for predicting phenotype from human samples.

We tested whether polydatin leads to community remodeling in complex human communities *in vivo*. Using a similar experimental scheme as for the defined community (Figure 7A), we colonized mice with two different human communities displaying different levels of resveratrol reduction *in vivo*: MV20, characterized by high levels of *Aequ_2118* and little accumulation of resveratrol after polydatin administration in mice, and MV18, characterized by low levels of *Aequ_2118* and high levels of fecal resveratrol after polydatin administration (Figure 7D). Assessment of community disruption, as measured by β-diversity between the initial condition (0 h) and treated time points (6 and 9 h) each day during the control (PBS) and treatment (polydatin) phase ($\beta\text{-diversity}_{vs.\ 0\ h}$), revealed distinct community responses as predicted by *Aequ_2118* gene levels and polydatin metabolism. Specifically, the MV18 community (low *Aequ_2118*, high resveratrol) was disrupted during the polydatin treatment period compared with MV20 (Figure 7E) and compared with the PBS control period (Figure 7F), while the MV20 community (high *Aequ_2118*, low resveratrol) was not significantly disrupted during polydatin treatment compared with PBS treatment (Figure 7F). By examining taxa abundance at the genus and species level, we identified *Bacteroides* spp. (e.g., *B. uniformis*) that were depleted and *Aestuariispira* (Alphaproteobacteria) spp. (e.g., *A. insulae*) that expanded during polydatin treatment in MV18 colonized mice (Figures 7G and S7G). These observations are consistent with the predicted susceptibility of these taxa to growth inhibition by resveratrol. Furthermore, while *B. uniformis* was also present in mice colonized with the MV20 community, it did not change in abundance in this community during polydatin treatment (Figure 7G). Indeed, there were no species in MV20-colonized mice with significantly different abundance during polydatin vs. control treatment (Figure S7G). Together, these *in vitro* and *in vivo* studies demonstrate how interindividual variability in a specific family of resveratrol reductases can explain the response of a defined or complex community to the dietary xenobiotic polydatin.

DISCUSSION

While significant progress has been made in understanding the mechanisms by which medical drugs and dietary macronutrients interact with the gut microbiome, little is known about microbiome interactions with the vast diversity of small-molecule micronutrients present in food. Here, we take a systematic approach to map how these dietary xenobiotics affect the growth of gut commensals, are metabolized, and remodel community composition. Using these maps, we hypothesize and experimentally validate mechanisms by which community remodeling occurs: xenobiotics with antibiotic activity can result in depletion of susceptible taxa, while metabolic transformation of these compounds can result in detoxification and community protection. Conversely, we identify non-toxic parent compounds that are transformed into toxic forms by gut microbes, resulting in community remodeling.

Our results build on previous studies focused on the interaction between whole foods and the gut microbiome by taking a reductionist approach with purified compounds instead of complex mixtures and measuring interindividual variation in human microbiome communities instead of population aggregates. Notably, we observe transient changes in microbiome composition *in vivo* that necessitates frequent sampling after xenobiotic consumption. Similar temporary remodeling in community composition on the daily timescale has been observed in humans after fiber intake.[63] These observations will inform future studies dissecting the interaction of dietary xenobiotics on the gut microbiome.

Human studies show that stevioside,[52] resveratrol,[64] and hesperidin[50] can all alter microbiome composition, and there is interest in the role of these compounds in health. In the case of stevioside, interindividual variability in community remodeling is suggested to impact host glucose tolerance, as demonstrated by gut microbiome transplant studies.[52] Resveratrol has also been extensively studied for multiple potential health benefits, including anti-inflammatory, anti-oxidant, and anti-atherosclerosis properties. This compound exhibits poor bioavailability, and some studies have linked its benefits to gut microbiome remodeling.[51,65] In addition to identifying differences in community remodeling in response to polydatin that are dependent on the microbiome, we also demonstrate that microbial metabolism significantly alters serum levels of polydatin, resveratrol, dihydroresveratrol, and their respective metabolites. Resveratrol and dihydroresveratrol have differences in their bioactivities,[66,67] and gut community-specific

differences in serum levels of these compounds may thus impact these bioactivities. Interestingly, serum resveratrol levels were higher in mice containing *E. lenta*, while host metabolites of resveratrol were significantly lower in these mice. These differences may reflect differences in host metabolism of resveratrol that are dependent on the presence of dihydroresveratrol and/or *E. lenta*. Notably, most studies on the impact of resveratrol have been performed utilizing *in vitro* assays or conventional mice, while human trials fail to consistently demonstrate benefits from resveratrol.[65] These studies usually do not consider the role of the gut microbiome in metabolizing resveratrol to dihydroresveratrol nor the consequences of interindividual variability in this trait. It is possible that stratifying populations by their ability to metabolize dietary xenobiotics, for example, through the abundance of genes such as resveratrol reductase, will illuminate trends that are otherwise masked.

Personalized nutrition is increasingly appreciated to be an important component of human health. Toward developing these nutrition strategies, large-scale clinical trials have begun to dissect how interindividual variation in the gut microbiome correlates with the impact of diet on health.[21] Mechanistic studies that complement these correlations are required to fully realize the potential of using personalized nutrition for therapeutic intervention. The maps we have generated and mechanisms that they illuminate are one step toward this goal.

Limitations of the study

Our results illustrate that community composition remodeling can occur through the toxification and detoxification of dietary xenobiotics by microbial metabolism. However, we also note several instances where we cannot explain interindividual variation in community remodeling or the specific species that change in abundance in response to a given dietary xenobiotic. Several mechanisms are likely involved, including species that derive a growth benefit from using a dietary xenobiotic or its metabolites as a nutrient,[56,68] or bioaccumulation of xenobiotics in the absence of chemical transformation.[69] As observed for other perturbations to microbial communities, the response to perturbation likely depends on interspecies interactions such as resource competition and cross-feeding.[57,70] Multi-omics approaches[71] along with ecological models that integrate mechanisms for cross-protection and cross-sensitization could allow for more accurate prediction of compositional changes. Additionally, it should be noted that the xenobiotic concentrations used in this study are based on indirect estimates derived from calculations based on human ileostomy and fecal recovery data, as well as physiology-based pharmacokinetic modeling. Finally, while the use of pure compounds allows us to take a reductionist approach, future studies can build on these results to capture the contributions of the food matrix or interactions between multiple food components in shaping microbiome-diet interactions, as well as how diet-dependent changes in microbiome composition (and microbiome-dependent changes in gut and serum xenobiotic profiles) impact diverse aspects of host biology.

RESOURCE AVAILABILITY

Lead contact

Requests for further information and resources may be directed to and will be fulfilled by lead contact, Andrew Goodman (andrew.goodman@yale.edu).

Materials availability

All resources related to this study, including bacterial strains and plasmids, are available from the lead contact upon request.

Data and code availability

- Raw 16S sequencing data and *E. lenta* RNA-seq data have been deposited in the NCBI database and are publicly available. LC-MS data are available on MetaboLights.[72] All accession numbers are listed in the key resources table.
- This paper does not report original code.
- Any additional information required to reanalyze the data reported in this paper is available upon request.

ACKNOWLEDGMENTS

We thank L. Valle, D. Lazo, and N. Barry for their assistance with gnotobiotic mouse experiments; T. Wu and the Yale West Campus Analytical Core for LC-MS assistance; the Yale Center for Genome Analysis for sequencing services; and J. Crawford and Q. Wu for assistance with activity guided purification of resveratrol. We also thank E. Balskus and X. Dong for the genetic tools to manipulate *E. lenta* and *G. urolithinfaciens* and for helpful advice. We thank G. Wright for the gift of *E. coli ΔbamB ΔtolC*. Support for this work was provided by the National Institutes of Health grants R01 AT010014, R35 GM118159, and R01 DK133798; by the Gray Foundation (to A.L.G.); and by the Damon Runyon Cancer Research Foundation (to E.J.C.).

AUTHOR CONTRIBUTIONS

E.J.C. and A.L.G. conceived the study and wrote the paper. N.T.N. performed IC_{50} testing and *in silico* pharmacokinetic modeling. A.A.V. performed measurements of resveratrol and associated metabolites in serum. E.J.C. performed all other experiments.

DECLARATION OF INTERESTS

A.L.G. serves on the scientific advisory boards of Seres Therapeutics, Taconic Biosciences, and Piton Therapeutics.

STAR★METHODS

Detailed methods are provided in the online version of this paper and include the following:

- KEY RESOURCES TABLE
- EXPERIMENTAL MODEL AND STUDY PARTICIPANT DETAILS
  - Animal experiments
  - Bacterial culture conditions
  - Human fecal material
- METHOD DETAILS
  - Chemicals
  - Community remodeling and metabolism assays
  - Xenobiotic metabolism by individual species
  - *In vitro* growth assays
  - LC-MS analysis
  - Estimating colonic xenobiotic concentrations
  - Genomic DNA extraction and 16S amplification
  - 16S rRNA analysis
  - Generating extracts for toxification studies
  - qPCR for species and gene abundance
  - *E. lenta* cell free supernatants
  - *E. lenta* RNA-seq

SUPPLEMENTAL INFORMATION

Supplemental information can be found online at https://doi.org/10.1016/j.cell.2024.08.038.

Received: July 13, 2023
Revised: February 23, 2024
Accepted: August 20, 2024
Published: September 24, 2024

REFERENCES

1. Qin, J., Li, R., Raes, J., Arumugam, M., Burgdorf, K.S., Manichanh, C., Nielsen, T., Pons, N., Levenez, F., Yamada, T., et al. (2010). A human gut microbial gene catalogue established by metagenomic sequencing. Nature *464*, 59–65. https://doi.org/10.1038/nature08821.
2. Wang, Z., Klipfell, E., Bennett, B.J., Koeth, R., Levison, B.S., DuGar, B., Feldstein, A.E., Britt, E.B., Fu, X., Chung, Y.-M., et al. (2011). Gut flora metabolism of phosphatidylcholine promotes cardiovascular disease. Nature *472*, 57–63. https://doi.org/10.1038/nature09922.
3. Karlsson, F.H., Fåk, F., Nookaew, I., Tremaroli, V., Fagerberg, B., Petranovic, D., Bäckhed, F., and Nielsen, J. (2012). Symptomatic atherosclerosis is associated with an altered gut metagenome. Nat. Commun. *3*, 1245. https://doi.org/10.1038/ncomms2266.
4. Franzosa, E.A., Sirota-Madi, A., Avila-Pacheco, J., Fornelos, N., Haiser, H.J., Reinker, S., Vatanen, T., Hall, A.B., Mallick, H., McIver, L.J., et al. (2019). Gut microbiome structure and metabolic activity in inflammatory bowel disease. Nat. Microbiol. *4*, 293–305. https://doi.org/10.1038/s41564-018-0306-4.
5. Qin, J., Li, Y., Cai, Z., Li, S., Zhu, J., Zhang, F., Liang, S., Zhang, W., Guan, Y., Shen, D., et al. (2012). A metagenome-wide association study of gut microbiota in type 2 diabetes. Nature *490*, 55–60. https://doi.org/10.1038/nature11450.
6. Turnbaugh, P.J., Hamady, M., Yatsunenko, T., Cantarel, B.L., Duncan, A., Ley, R.E., Sogin, M.L., Jones, W.J., Roe, B.A., Affourtit, J.P., et al. (2009). A core gut microbiome in obese and lean twins. Nature *457*, 480–484. https://doi.org/10.1038/nature07540.
7. Gopalakrishnan, V., Helmink, B.A., Spencer, C.N., Reuben, A., and Wargo, J.A. (2018). The influence of the gut microbiome on cancer, immunity, and cancer immunotherapy. Cancer Cell *33*, 570–580. https://doi.org/10.1016/j.ccell.2018.03.015.
8. Irigaray, P., Newby, J.A., Clapp, R., Hardell, L., Howard, V., Montagnier, L., Epstein, S., and Belpomme, D. (2007). Lifestyle-related factors and environmental agents causing cancer: An overview. Biomed. Pharmacother. *61*, 640–658. https://doi.org/10.1016/j.biopha.2007.10.006.
9. Zeevi, D., Korem, T., Zmora, N., Israeli, D., Rothschild, D., Weinberger, A., Ben-Yacov, O., Lador, D., Avnit-Sagi, T., Lotan-Pompan, M., et al. (2015). Personalized nutrition by prediction of glycemic responses. Cell *163*, 1079–1094. https://doi.org/10.1016/j.cell.2015.11.001.
10. World Cancer Research Fund/American Institute for Cancer Research (2018). Diet, nutrition, physical activity and cancer: a global perspective. https://www.wcrf.org/wp-content/uploads/2021/02/Summary-of-Third-Expert-Report-2018.pdf.
11. Berry, S.E., Valdes, A.M., Drew, D.A., Asnicar, F., Mazidi, M., Wolf, J., Capdevila, J., Hadjigeorgiou, G., Davies, R., Al Khatib, H., et al. (2020). Human postprandial responses to food and potential for precision nutrition. Nat. Med. *26*, 964–973. https://doi.org/10.1038/s41591-020-0934-0.
12. Rothschild, D., Weissbrod, O., Barkan, E., Kurilshikov, A., Korem, T., Zeevi, D., Costea, P.I., Godneva, A., Kalka, I.N., Bar, N., et al. (2018). Environment dominates over host genetics in shaping human gut microbiota. Nature *555*, 210–215. https://doi.org/10.1038/nature25973.
13. Wu, G.D., Chen, J., Hoffmann, C., Bittinger, K., Chen, Y.-Y., Keilbaugh, S.A., Bewtra, M., Knights, D., Walters, W.A., Knight, R., et al. (2011). Linking long-term dietary patterns with gut microbial enterotypes. Science *334*, 105–108. https://doi.org/10.1126/science.1208344.
14. Walker, A.W., Ince, J., Duncan, S.H., Webster, L.M., Holtrop, G., Ze, X., Brown, D., Stares, M.D., Scott, P., Bergerat, A., et al. (2011). Dominant and diet-responsive groups of bacteria within the human colonic microbiota. ISME J. *5*, 220–230. https://doi.org/10.1038/ismej.2010.118.
15. David, L.A., Maurice, C.F., Carmody, R.N., Gootenberg, D.B., Button, J.E., Wolfe, B.E., Ling, A.V., Devlin, A.S., Varma, Y., Fischbach, M.A., et al. (2014). Diet rapidly and reproducibly alters the human gut microbiome. Nature *505*, 559–563. https://doi.org/10.1038/nature12820.
16. Basak, S., Banerjee, A., Pathak, S., and Duttaroy, A.K. (2022). Dietary fats and the gut microbiota: their impacts on lipid-induced metabolic syndrome. J. Funct. Foods *91*, 105026. https://doi.org/10.1016/j.jff.2022.105026.
17. Zhao, J., Zhang, X., Liu, H., Brown, M.A., and Qiao, S. (2019). Dietary protein and gut microbiota composition and function. Curr. Protein Pept. Sci. *20*, 145–154. https://doi.org/10.2174/1389203719666180514145437.
18. Koropatkin, N.M., Cameron, E.A., and Martens, E.C. (2012). How glycan metabolism shapes the human gut microbiota. Nat. Rev. Microbiol. *10*, 323–335. https://doi.org/10.1038/nrmicro2746.
19. Delannoy-Bruno, O., Desai, C., Raman, A.S., Chen, R.Y., Hibberd, M.C., Cheng, J., Han, N., Castillo, J.J., Couture, G., Lebrilla, C.B., et al. (2021). Evaluating microbiome-directed fibre snacks in gnotobiotic mice and humans. Nature *595*, 91–95. https://doi.org/10.1038/s41586-021-03671-4.
20. Cantu-Jungles, T.M., and Hamaker, B.R. (2020). New view on dietary fiber selection for predictable shifts in gut microbiota. mBio *11*, e02179-19. https://doi.org/10.1128/mBio.02179-19.
21. Hernández-Calderón, P., Wiedemann, L., and Benítez-Páez, A. (2022). The microbiota composition drives personalized nutrition: gut microbes as predictive biomarkers for the success of weight loss diets. Front. Nutr. *9*, 1006747. https://doi.org/10.3389/fnut.2022.1006747.
22. Turnbaugh, P.J., Ley, R.E., Mahowald, M.A., Magrini, V., Mardis, E.R., and Gordon, J.I. (2006). An obesity-associated gut microbiome with increased capacity for energy harvest. Nature *444*, 1027–1031. https://doi.org/10.1038/nature05414.
23. Liu, Y., Chen, H., Van Treuren, W., Hou, B.-H., Higginbottom, S.K., and Dodd, D. (2022). *Clostridium sporogenes* uses reductive Stickland metabolism in the gut to generate ATP and produce circulating metabolites. Nat. Microbiol. *7*, 695–706. https://doi.org/10.1038/s41564-022-01109-9.
24. Koppel, N., Maini Rekdal, V., and Balskus, E.P. (2017). Chemical transformation of xenobiotics by the human gut microbiota. Science *356*, eaag2770. https://doi.org/10.1126/science.aag2770.
25. Barabási, A.-L., Menichetti, G., and Loscalzo, J. (2019). The unmapped chemical complexity of our diet. Nat. Food *1*, 33–37. https://doi.org/10.1038/s43016-019-0005-1.
26. Valdés, L., Cuervo, A., Salazar, N., Ruas-Madiedo, P., Gueimonde, M., and González, S. (2015). The relationship between phenolic compounds from diet and microbiota: impact on human health. Food Funct. *6*, 2424–2439. https://doi.org/10.1039/C5FO00322A.
27. Catalkaya, G., Venema, K., Lucini, L., Rocchetti, G., Delmas, D., Daglia, M., De Filippis, A., Xiao, H., Quiles, J.L., Xiao, J., et al. (2020). Interaction of dietary polyphenols and gut microbiota: Microbial metabolism of polyphenols, influence on the gut microbiota, and implications on host health. Food Front. *1*, 109–133. https://doi.org/10.1002/fft2.25.
28. Dueñas, M., Muñoz-González, I., Cueva, C., Jiménez-Girón, A., Sánchez-Patán, F., Santos-Buelga, C., Moreno-Arribas, M.V., and Bartolomé, B.

(2015). A survey of modulation of gut microbiota by dietary polyphenols. BioMed Res. Int. *2015*, 850902. https://doi.org/10.1155/2015/850902.

29. Lee, H.C., Jenner, A.M., Low, C.S., and Lee, Y.K. (2006). Effect of tea phenolics and their aromatic fecal bacterial metabolites on intestinal microbiota. Res. Microbiol. *157*, 876–884. https://doi.org/10.1016/j.resmic.2006.07.004.

30. Rodríguez-Daza, M.C., Pulido-Mateos, E.C., Lupien-Meilleur, J., Guyonnet, D., Desjardins, Y., and Roy, D. (2021). Polyphenol-mediated gut microbiota modulation: toward prebiotics and further. Front. Nutr. *8*, 689456. https://doi.org/10.3389/fnut.2021.689456.

31. Estruel-Amades, S., Massot-Cladera, M., Pérez-Cano, F.J., Franch, À., Castell, M., and Camps-Bossacoma, M. (2019). Hesperidin effects on gut microbiota and gut-associated lymphoid tissue in healthy rats. Nutrients *11*, 324. https://doi.org/10.3390/nu11020324.

32. Zhang, J., Empl, M.T., Schwab, C., Fekry, M.I., Engels, C., Schneider, M., Lacroix, C., Steinberg, P., and Sturla, S.J. (2017). Gut microbial transformation of the dietary imidazoquinoxaline mutagen MeIQx reduces its cytotoxic and mutagenic potency. Toxicol. Sci. *159*, 266–276. https://doi.org/10.1093/toxsci/kfx132.

33. Kenny, D.J., Plichta, D.R., Shungin, D., Koppel, N., Hall, A.B., Fu, B., Vasan, R.S., Shaw, S.Y., Vlamakis, H., Balskus, E.P., et al. (2020). Cholesterol metabolism by uncultured human gut bacteria influences host cholesterol level. Cell Host Microbe *28*, 245–257.e6. https://doi.org/10.1016/j.chom.2020.05.013.

34. Maier, L., Pruteanu, M., Kuhn, M., Zeller, G., Telzerow, A., Anderson, E.E., Brochado, A.R., Fernandez, K.C., Dose, H., Mori, H., et al. (2018). Extensive impact of non-antibiotic drugs on human gut bacteria. Nature *555*, 623–628. https://doi.org/10.1038/nature25979.

35. Zimmermann, M., Zimmermann-Kogadeeva, M., Wegmann, R., and Goodman, A.L. (2019). Mapping human microbiome drug metabolism by gut bacteria and their genes. Nature *570*, 462–467. https://doi.org/10.1038/s41586-019-1291-3.

36. Javdan, B., Lopez, J.G., Chankhamjon, P., Lee, Y.-C.J., Hull, R., Wu, Q., Wang, X., Chatterjee, S., and Donia, M.S. (2020). Personalized Mapping of Drug Metabolism by the Human Gut Microbiome. Cell *181*, 1661–1679.e22. https://doi.org/10.1016/j.cell.2020.05.001.

37. Zhang, X., Han, Y., Huang, W., Jin, M., and Gao, Z. (2021). The influence of the gut microbiota on the bioavailability of oral drugs. Acta Pharm. Sin. B *11*, 1789–1812. https://doi.org/10.1016/j.apsb.2020.09.013.

38. Ellenbogen, J.B., Jiang, R., Kountz, D.J., Zhang, L., and Krzycki, J.A. (2021). The MttB superfamily member MtyB from the human gut symbiont *Eubacterium limosum* is a cobalamin-dependent γ-butyrobetaine methyltransferase. J. Biol. Chem. *297*, 101327. https://doi.org/10.1016/j.jbc.2021.101327.

39. Xie, Y., Yang, W., Tang, F., Chen, X., and Ren, L. (2015). Antibacterial activities of flavonoids: structure-activity relationship and mechanism. Curr. Med. Chem. *22*, 132–149. https://doi.org/10.2174/0929867321666140916113443.

40. Xu, M., Wu, P., Shen, F., Ji, J., and Rakesh, K.P. (2019). Chalcone derivatives and their antibacterial activities: current development. Bioorg. Chem. *91*, 103133. https://doi.org/10.1016/j.bioorg.2019.103133.

41. Singh, D., Mendonsa, R., Koli, M., Subramanian, M., and Nayak, S.K. (2019). Antibacterial activity of resveratrol structural analogues: A mechanistic evaluation of the structure-activity relationship. Toxicol. Appl. Pharmacol. *367*, 23–32. https://doi.org/10.1016/j.taap.2019.01.025.

42. Déprez, S., Brezillon, C., Rabot, S., Philippe, C., Mila, I., Lapierre, C., and Scalbert, A. (2000). Polymeric proanthocyanidins are catabolized by human colonic microflora into low-molecular-weight phenolic acids. J. Nutr. *130*, 2733–2738. https://doi.org/10.1093/jn/130.11.2733.

43. Hollman, P.C.H. (2009). Absorption, Bioavailability, and Metabolism of Flavonoids. Pharm. Biol. *42*, 74–83. https://doi.org/10.3109/13880200490893492.

44. Hollman, P.C.H., De Vries, J.H.M., Van Leeuwen, S.D., Mengelers, M.J.B., and Katan, M.B. (1995). Absorption of dietary quercetin glycosides and quercetin in healthy ileostomy volunteers. Am. J. Clin. Nutr. *62*, 1276–1282. https://doi.org/10.1093/AJCN/62.6.1276.

45. Hollman, P.C.H., Van Trijp, J.M.P., Buysman, M.N.C.P., van der Gaag, M.S., Mengelers, M.J.B., De Vries, J.H.M., and Katan, M.B. (1997). Relative bioavailability of the antioxidant flavonoid quercetin from various foods in man. FEBS Lett. *418*, 152–156. https://doi.org/10.1016/S0014-5793(97)01367-7.

46. Scalbert, A., and Williamson, G. (2000). Dietary intake and bioavailability of polyphenols. J. Nutr. *130*, 2073S–2085S. https://doi.org/10.1093/jn/130.8.2073S.

47. Nielsen, I.L.F., Chee, W.S.S., Poulsen, L., Offord-Cavin, E., Rasmussen, S.E., Frederiksen, H., Enslen, M., Barron, D., Horcajada, M.N., and Williamson, G. (2006). Bioavailability Is Improved by Enzymatic Modification of the Citrus Flavonoid Hesperidin in Humans: A Randomized, Double-Blind, Crossover Trial. J. Nutr. *136*, 404–408. https://doi.org/10.1093/JN/136.2.404.

48. Kelly, C.J., Verdegaal, A.A., Anderson, B.W., Shaw, W.L., Bencivenga-Barry, N.A., Folta-Stogniew, E., and Goodman, A.L. (2023). Metformin inhibits digestive proteases and impairs protein digestion in mice. J. Biol. Chem. *299*, 105363. https://doi.org/10.1016/J.JBC.2023.105363.

49. King, A.M., Reid-Yu, S.A., Wang, W., King, D.T., De Pascale, G., Strynadka, N.C., Walsh, T.R., Coombes, B.K., and Wright, G.D. (2014). Aspergillomarasmine A overcomes metallo-β-lactamase antibiotic resistance. Nature *510*, 503–506. https://doi.org/10.1038/nature13445.

50. Fidélix, M., Milenkovic, D., Sivieri, K., and Cesar, T. (2020). Microbiota modulation and effects on metabolic biomarkers by orange juice: a controlled clinical trial. Food Funct. *11*, 1599–1610. https://doi.org/10.1039/c9fo02623a.

51. Chen, M.L., Yi, L., Zhang, Y., Zhou, X., Ran, L., Yang, J., Zhu, J.D., Zhang, Q.Y., and Mi, M.T. (2016). Resveratrol attenuates trimethylamine- N-Oxide (TMAO)-induced atherosclerosis by regulating TMAO synthesis and bile acid metabolism via remodeling of the gut microbiota. mBio *7*, e02210-15. https://doi.org/10.1128/mBio.02210-15.

52. Suez, J., Cohen, Y., Valdés-Mas, R., Mor, U., Dori-Bachash, M., Federici, S., Zmora, N., Leshem, A., Heinemann, M., Linevsky, R., et al. (2022). Personalized microbiome-driven effects of non-nutritive sweeteners on human glucose tolerance. Cell *185*, 3307–3328.e19. https://doi.org/10.1016/j.cell.2022.07.016.

53. Bode, L.M., Bunzel, D., Huch, M., Cho, G.-S., Ruhland, D., Bunzel, M., Bub, A., Franz, C.M.A.P., and Kulling, S.E. (2013). In vivo and in vitro metabolism of trans-resveratrol by human gut microbiota. Am. J. Clin. Nutr. *97*, 295–309. https://doi.org/10.3945/ajcn.112.049379.

54. Braune, A., Gütschow, M., and Blaut, M. (2019). An NADH-dependent reductase from *Eubacterium ramulus* catalyzes the stereospecific heteroring cleavage of flavanones and flavanonols. Appl. Environ. Microbiol. *85*, e01233-19. https://doi.org/10.1128/AEM.01233-19.

55. Braune, A., and Blaut, M. (2016). Bacterial species involved in the conversion of dietary flavonoids in the human gut. Gut Microbes *7*, 216–234. https://doi.org/10.1080/19490976.2016.1158395.

56. Simmering, R., Pforte, H., Jacobasch, G., and Blaut, M. (2002). The growth of the flavonoid-degrading intestinal bacterium, *Eubacterium ramulus*, is stimulated by dietary flavonoids in vivo. FEMS Microbiol. Ecol. *40*, 243–248. https://doi.org/10.1111/J.1574-6941.2002.TB00957.X.

57. Newton, D.P., Ho, P.-Y., and Huang, K.C. (2023). Modulation of antibiotic effects on microbial communities by resource competition. Nat. Commun. *14*, 2398. https://doi.org/10.1038/s41467-023-37895-x.

58. Ossowicki, A., Raaijmakers, J.M., and Garbeva, P. (2021). Disentangling soil microbiome functions by perturbation. Environ. Microbiol. Rep. *13*, 582–590. https://doi.org/10.1111/1758-2229.12989.

59. Weiss, A.S., Niedermeier, L.S., von Strempel, A., Burrichter, A.G., Ring, D., Meng, C., Kleigrewe, K., Lincetto, C., Hübner, J., and Stecher, B. (2023). Nutritional and host environments determine community ecology and

keystone species in a synthetic gut bacterial community. Nat. Commun. *14*, 4780. https://doi.org/10.1038/S41467-023-40372-0.

60. Weiss, A.S., Burrichter, A.G., Durai Raj, A.C., von Strempel, A., Meng, C., Kleigrewe, K., Münch, P.C., Rössler, L., Huber, C., Eisenreich, W., et al. (2022). In vitro interaction network of a synthetic gut bacterial community. ISME J. *16*, 1095–1109. https://doi.org/10.1038/S41396-021-01153-Z.
61. Dong, X., Guthrie, B.G.H., Alexander, M., Noecker, C., Ramirez, L., Glasser, N.R., Turnbaugh, P.J., and Balskus, E.P. (2022). Genetic manipulation of the human gut bacterium *Eggerthella lenta* reveals a widespread family of transcriptional regulators. Nat. Commun. *13*, 7624. https://doi.org/10.1038/s41467-022-33576-3.
62. Light, S.H., Méheust, R., Ferrell, J.L., Cho, J., Deng, D., Agostoni, M., Iavarone, A.T., Banfield, J.F., D'Orazio, S.E.F., and Portnoy, D.A. (2019). Extracellular electron transfer powers flavinylated extracellular reductases in Gram-positive bacteria. Proc. Natl. Acad. Sci. USA *116*, 26892–26899. https://doi.org/10.1073/pnas.1915678116.
63. David, L.A., Materna, A.C., Friedman, J., Campos-Baptista, M.I., Blackburn, M.C., Perrotta, A., Erdman, S.E., and Alm, E.J. (2014). Host lifestyle affects human microbiota on daily timescales. Genome Biol. *15*, R89. https://doi.org/10.1186/gb-2014-15-7-r89.
64. Queipo-Ortuño, M.I., Boto-Ordóñez, M., Murri, M., Gomez-Zumaquero, J.M., Clemente-Postigo, M., Estruch, R., Cardona Diaz, F., Andrés-Lacueva, C., and Tinahones, F.J. (2012). Influence of red wine polyphenols and ethanol on the gut microbiota ecology and biochemical biomarkers. Am. J. Clin. Nutr. *95*, 1323–1334. https://doi.org/10.3945/ajcn.111.027847.
65. Inchingolo, A.D., Malcangi, G., Inchingolo, A.M., Piras, F., Settanni, V., Garofoli, G., Palmieri, G., Ceci, S., Patano, A., De Leonardis, N., et al. (2022). Benefits and implications of resveratrol supplementation on microbiota modulations: A systematic review of the literature. Int. J. Mol. Sci. *23*, 4027. https://doi.org/10.3390/ijms23074027.
66. Li, F., Han, Y., Wu, X., Cao, X., Gao, Z., Sun, Y., Wang, M., and Xiao, H. (2022). Gut Microbiota-Derived Resveratrol Metabolites, Dihydroresveratrol and Lunularin, Significantly Contribute to the Biological Activities of Resveratrol. Front. Nutr. *9*, 912591. https://doi.org/10.3389/FNUT.2022.912591.
67. Poór, M., Kaci, H., Bodnárová, S., Mohos, V., Fliszár-Nyúl, E., Kunsági-Máté, S., Özvegy-Laczka, C., and Lemli, B. (2022). Interactions of resveratrol and its metabolites (resveratrol-3-sulfate, resveratrol-3-glucuronide, and dihydroresveratrol) with serum albumin, cytochrome P450 enzymes, and OATP transporters. Biomed. Pharmacother. *151*, 113136. https://doi.org/10.1016/J.BIOPHA.2022.113136.
68. Maini Rekdal, V., Bess, E.N., Bisanz, J.E., Turnbaugh, P.J., and Balskus, E.P. (2019). Discovery and inhibition of an interspecies gut bacterial pathway for Levodopa metabolism. Science *364*, eaau6323. https://doi.org/10.1126/science.aau6323.
69. Klünemann, M., Andrejev, S., Blasche, S., Mateus, A., Phapale, P., Devendran, S., Vappiani, J., Simon, B., Scott, T.A., Kafkia, E., et al. (2021). Bioaccumulation of therapeutic drugs by human gut bacteria. Nature *597*, 533–538. https://doi.org/10.1038/s41586-021-03891-8.
70. Patnode, M.L., Beller, Z.W., Han, N.D., Cheng, J., Peters, S.L., Terrapon, N., Henrissat, B., Le Gall, S., Saulnier, L., Hayashi, D.K., et al. (2019). Interspecies competition impacts targeted manipulation of human gut bacteria by fiber-derived glycans. Cell *179*, 59–73.e13. https://doi.org/10.1016/J.CELL.2019.08.011.
71. Wuyts, S., Alves, R., Zimmermann-Kogadeeva, M., Nishijima, S., Blasche, S., Driessen, M., Geyer, P.E., Hercog, R., Kartal, E., Maier, L., et al. (2023). Consistency across multi-omics layers in a drug-perturbed gut microbial community. Mol. Syst. Biol. *19*, e11525. https://doi.org/10.15252/MSB.202311525.
72. Yurekten, O., Payne, T., Tejera, N., Amaladoss, F.X., Martin, C., Williams, M., and O'Donovan, C. (2023). MetaboLights: open data repository for metabolomics. Nucleic Acids Res. *52*, D640–D646. https://doi.org/10.1093/NAR/GKAD1045.
73. Tawk, C., Lim, B., Bencivenga-Barry, N.A., Lees, H.J., Ramos, R.J.F., Cross, J., and Goodman, A.L. (2023). Infection leaves a genetic and functional mark on the gut population of a commensal bacterium. Cell Host Microbe *31*, 811–826.e6. https://doi.org/10.1016/j.chom.2023.04.005.
74. Baba, T., Ara, T., Hasegawa, M., Takai, Y., Okumura, Y., Baba, M., Datsenko, K.A., Tomita, M., Wanner, B.L., and Mori, H. (2006). Construction of Escherichia coli K-12 in-frame, single-gene knockout mutants: the Keio collection. Mol. Syst. Biol. *2*, 2006.0008. https://doi.org/10.1038/MSB4100050.
75. Bolyen, E., Rideout, J.R., Dillon, M.R., Bokulich, N.A., Abnet, C.C., Al-Ghalith, G.A., Alexander, H., Alm, E.J., Arumugam, M., Asnicar, F., et al. (2019). Reproducible, interactive, scalable and extensible microbiome data science using QIIME 2. Nat. Biotechnol. *37*, 852–857. https://doi.org/10.1038/s41587-019-0209-9.
76. Langmead, B., and Salzberg, S.L. (2012). Fast gapped-read alignment with Bowtie 2. Nat. Methods *9*, 357–359. https://doi.org/10.1038/nmeth.1923.
77. Liao, Y., Smyth, G.K., and Shi, W. (2019). The R package Rsubread is easier, faster, cheaper and better for alignment and quantification of RNA sequencing reads. Nucleic Acids Res. *47*, e47. https://doi.org/10.1093/nar/gkz114.
78. Love, M.I., Huber, W., and Anders, S. (2014). Moderated estimation of fold change and dispersion for RNA-seq data with DESeq2. Genome Biol. *15*, 550. https://doi.org/10.1186/s13059-014-0550-8.
79. Goodman, A.L., McNulty, N.P., Zhao, Y., Leip, D., Mitra, R.D., Lozupone, C.A., Knight, R., and Gordon, J.I. (2009). Identifying Genetic Determinants Needed to Establish a Human Gut Symbiont in Its Habitat. Cell Host Microbe *6*, 279–289. https://doi.org/10.1016/j.chom.2009.08.003.
80. Zimmermann, M., Zimmermann-Kogadeeva, M., Wegmann, R., and Goodman, A.L. (2019). Separating host and microbiome contributions to drug pharmacokinetics and toxicity. Science *363*, eaat9931. https://doi.org/10.1126/science.aat9931.
81. Folz, J., Culver, R.N., Morales, J.M., Grembi, J., Triadafilopoulos, G., Relman, D.A., Huang, K.C., Shalon, D., and Fiehn, O. (2023). Human metabolome variation along the upper intestinal tract. Nat. Metab. *5*, 777–788. https://doi.org/10.1038/s42255-023-00777-z.
82. Yan, K., Hung, A., Parmer, C., Yang, H., Jain, D., Lim, B., Goodman, A.L., and Garcia-Tsao, G. (2021). Obeticholic acid decreases intestinal content of enterococcus in rats with cirrhosis and ascites. Hepatol. Commun. *5*, 1507–1517. https://doi.org/10.1002/hep4.1740.
83. Kozich, J.J., Westcott, S.L., Baxter, N.T., Highlander, S.K., and Schloss, P.D. (2013). Development of a dual-index sequencing strategy and curation pipeline for analyzing amplicon sequence data on the MiSeq Illumina sequencing platform. Appl. Environ. Microbiol. *79*, 5112–5120. https://doi.org/10.1128/AEM.01043-13.
84. McDonald, D., Clemente, J.C., Kuczynski, J., Rideout, J.R., Stombaugh, J., Wendel, D., Wilke, A., Huse, S., Hufnagle, J., Meyer, F., et al. (2012). The Biological Observation Matrix (BIOM) format or: how I learned to stop worrying and love the ome-ome. Gigascience *1*, 7. https://doi.org/10.1186/2047-217X-1-7.
85. Hamady, M., Walker, J.J., Harris, J.K., Gold, N.J., and Knight, R. (2008). Error-correcting barcoded primers for pyrosequencing hundreds of samples in multiplex. Nat. Methods *5*, 235–237. https://doi.org/10.1038/nmeth.1184.
86. Hamady, M., and Knight, R. (2009). Microbial community profiling for human microbiome projects: Tools, techniques, and challenges. Genome Res. *19*, 1141–1152. https://doi.org/10.1101/gr.085464.108.
87. Callahan, B.J., McMurdie, P.J., Rosen, M.J., Han, A.W., Johnson, A.J.A., and Holmes, S.P. (2016). DADA2: High-resolution sample inference from Illumina amplicon data. Nat. Methods *13*, 581–583. https://doi.org/10.1038/nmeth.3869.
88. Rekdal, V.M., Bernadino, P.N., Luescher, M.U., Kiamehr, S., Le, C., Bisanz, J.E., Turnbaugh, P.J., Bess, E.N., and Balskus, E.P. (2020). A widely

distributed metalloenzyme class enables gut microbial metabolism of host-and diet-derived catechols. eLife *9*, e50845. https://doi.org/10.7554/ELIFE.50845.

89. Bisanz, J.E., Soto-Perez, P., Noecker, C., Aksenov, A.A., Lam, K.N., Kenney, G.E., Bess, E.N., Haiser, H.J., Kyaw, T.S., Yu, F.B., et al. (2020). A genomic toolkit for the mechanistic dissection of intractable human gut bacteria. Cell Host Microbe *27*, 1001–1013.e9. https://doi.org/10.1016/j.chom.2020.04.006.
90. Olson, R.D., Assaf, R., Brettin, T., Conrad, N., Cucinell, C., Davis, J.J., Dempsey, D.M., Dickerman, A., Dietrich, E.M., Kenyon, R.W., et al. (2023). Introducing the bacterial and viral bioinformatics resource center (BV-BRC): a resource combining PATRIC, IRD and ViPR. Nucleic Acids Res. *51*, D678–D689. https://doi.org/10.1093/nar/gkac1003.
91. Bess, E.N., Bisanz, J.E., Yarza, F., Bustion, A., Rich, B.E., Li, X., Kitamura, S., Waligurski, E., Ang, Q.Y., Alba, D.L., et al. (2020). Genetic basis for the cooperative bioactivation of plant lignans by *Eggerthella lenta* and other human gut bacteria. Nat. Microbiol. *5*, 56–66. https://doi.org/10.1038/s41564-019-0596-1.
92. Senizza, A., Rocchetti, G., Mosele, J.I., Patrone, V., Callegari, M.L., Morelli, L., and Lucini, L. (2020). Lignans and gut microbiota: An interplay revealing potential health implications. Molecules *25*, 5709. https://doi.org/10.3390/molecules25235709.
93. Selma, M.V., Beltrán, D., García-Villalba, R., Espín, J.C., and Tomás-Barberán, F.A. (2014). Description of urolithin production capacity from ellagic acid of two human intestinal *Gordonibacter* species. Food Funct. *5*, 1779–1784. https://doi.org/10.1039/C4FO00092G.
94. Tomás-Barberán, F.A., García-Villalba, R., González-Sarrías, A., Selma, M.V., and Espín, J.C. (2014). Ellagic acid metabolism by human gut microbiota: consistent observation of three urolithin phenotypes in intervention trials, independent of food source, age, and health status. J. Agric. Food Chem. *62*, 6535–6538. https://doi.org/10.1021/jf5024615.

STAR★METHODS

KEY RESOURCES TABLE

REAGENT or RESOURCE	SOURCE	IDENTIFIER
Bacterial and virus strains		
Strains used in this study	See Table S2	N/A
Escherichia coli ΔbamB ΔtolC	Wright lab, McMaster University	Reference King et al.[49]
Bacteroides thetaiotaomicron Δtdk att1::pNBU2-BC1	Goodman lab, Yale University	Reference Tawk et al.[73]
Escherichia coli JW0333	Keio collection	Reference Baba et al. [74]
Chemicals, peptides, and recombinant proteins		
Dietary xenobiotics	See Table S1	N/A
GAM Broth Modified	HyServe	Cat# 5433
Bryant and Burkey Medium	VWR	Cat# 95021-064
Bacto Brain Heart Infusion	VWR	Cat# 237500
Defibrinated Horse Blood	Quad Five	Cat# 210-1000
Breathe-Easy sealing membrane	Sigma	Cat# Z380059-1PAK
KAPA Sybr Fast Universal	KAPA Biosystems	Cat# KK4602
Zirconia-Silica Bead, 0.1mm	BioSpec	Cat# 11079101z
Phenol – chloroform – isoamyl alcohol mixture	Sigma	Cat# 77617-500ML
E-Z 96 Cycle Pure Kit	Omega	Cat# D1043
TRIzol reagent	Thermofisher	Cat# 15596018
SequalPrep Normalization Plate Kit, 96-well	Invitrogen	Cat# A1051001
AccuPrime Pfx SuperMix	Invitrogen	Cat# 12344040
RNAprotect Bacteria Reagent	Qiagen	Cat# 76506
RNeasy Mini Kit	Qiagen	Cat# 74106
DNA-*free* DNA Removal Kit	Thermofisher	Cat# AM1906
NEBNext rRNA Depletion Kit	NEB	Cat# E7850S
Ultra II Directional Library Prep Kit for Illumina	NEB	Cat# E7760S
T4 polynucleotide kinase	NEB	Cat# M0201S
Cumate (4-Isopropylbenzoic acid)	Sigma	Cat# 268402
LabDiet JL Rat and Mouse/Auto 6F	Purina	Cat# 5K67
Kinetex 1.7 μm EVO C18 100 Å, LC Column 100 x 2.1 mm, EA	Phenomenex	Cat# 00D-4726-AN
HyperSep Retain PEP 30 mg/1 mL 96 Removable Well Plate	Thermofisher	Cat# 60303-207
Critical commercial assays		
Quant-IT PicoGreen dsDNA assay kit	Invitrogen	Cat# P7589
Deposited data		
RNA-seq: Transcriptomic analysis of Eggerthella lenta response to resveratrol	NCBI SRA: PRJNA992521	
16S sequencing: Effect of dietary xenobiotics on gut microbiome composition - 161 dietary xenobiotics	NCBI SRA: PRJNA992071	
16S sequencing: Effect of dietary xenobiotics on gut microbiome composition - polydatin and resveratrol	NCBI SRA: PRJNA992066	

(*Continued on next page*)

Continued

REAGENT or RESOURCE	SOURCE	IDENTIFIER
16S sequencing: Effect of dietary xenobiotics on gut microbiome composition - in vivo	NCBI SRA: PRJNA992060	
LC-MS Metabolism Data	Metabolights: MTBLS9221	
Experimental models: Organisms/strains		
Mouse: C57BL/6NTac Germ-free	Taconic	Model# GF-B6
Oligonucleotides		
See Table S7 for oligonucleotides	This study	N/A
Recombinant DNA		
pXD68Kan2-AphA	Addgene	Cat# 191248
pXD71Cas10RFP-Pct5.1-crRNA(Aarl)-RFP	Addgene	Cat# 192273
pXD70Tet(LacZ3)	Balskus Laboratory, Harvard University	Reference Dong et al.[61]
pXD68-288-289	This study	N/A
pXD71Cas10-crRNA-288	This study	N/A
pXD71Cas10-crRNA-1283-5	This study	N/A
Software and algorithms		
MassHunter Quantitative Analysis Software	Agilent	Version 7
ADMET Predictor	Simulations Plus	Version 10.4
GastroPlus	Simulations Plus	Version 9.8.2
QIIME	Bolyen et al.[75]	Version 1.8
QIIME2	Bolyen et al.[75]	Version 2020.11
Bowtie2	Langmead and Salzberg et al.[76]	Version 2.4.2
Rsubread	Liao et al.[77]	Version 2.14.2
DESeq2	Love et al.[78]	Version 1.40.1
Prism	Graphpad	Version 9
Spotfire	Tibco	Version 6.5.1

EXPERIMENTAL MODEL AND STUDY PARTICIPANT DETAILS

Animal experiments

All mice experiments were performed using protocols approved by the Yale University Institutional Animal Care and Use Committee (IACUC). Germ-free C57BL/6 mice (7-12 weeks old) were used in this study. A mix of both sexes were used for all studies. In experiments examining dietary xenobiotic metabolism, animals were housed alone or with a partner in gnotobiotic isocages (Sentry Sealed Positive Pressure (SPP) isolation cage system (Allentown, Inc., Allentown, NJ, USA)). No differences between individually versus co-housed mice were observed. In experiments examining community disruption, mice carrying the same bacterial community were individually housed in flexible plastic gnotobiotic isolators. Mice were kept in a 12 hr light/dark cycle and provided a standard, autoclaved mouse chow (5K67 LabDiet, Purina) ad libitum, and autoclaved water for the duration of the experiment. The levels of the studied dietary xenobiotics were below the level of detection in the mouse chow, as quantified by LC-MS.

Bacterial culture conditions

A flexible anaerobic chamber (Coy Laboratory Products) containing 20% CO_2, 10% H_2 and 70% N_2 and incubation at 37°C was used for all anaerobic microbiology steps. All anaerobic steps were performed using pre-reduced media and materials. Bacterial strains and culture conditions are listed in Table S2. Routine culturing in monoculture was performed in liquid mega medium,[79] or Brain Heart Infusion medium (BHI; Becton Dickinson) supplemented with 0.5 g/L cysteine, 10 g/L arginine, 1 mg/L vitamin K1 and 5 mg/L hemin (BHI++), as indicated. Experiments involving microbial communities were performed in a mixture of Bryant and Burkey Medium (BB; HiMedia) and Modified Gifu Anaerobic Medium (mGAM; HyServe) at a ratio of 7:3, herein referred to as BB:mGAM, as previously described.[36] For growth curve assays, additions to mGAM were made as indicated (Table S2), including mGAM+sugar (0.1% cellobiose, 0.1% fructose, 0.1% maltose). *E. coli* Top10 was used for molecular cloning and grown aerobically at 37°C in LB medium (200 rpm shaking) or LB agar supplemented with antibiotics as appropriate (50 μg/mL kanamycin, 100 μg/mL ampicillin). *E. lenta* and *G. urolithinfaciens* were routinely grown in BHI broth or agar containing 1% arginine and 10 mM sodium formate (BHIrf), supplemented with antibiotics as necessary (100 μg/mL kanamycin), unless otherwise indicated.

For community composition experiments where CFU were enumerated, strains with additional selective markers were utilized: *Bacteroides thetaiotaomicron Δtdk att1::pNBU2-BC1* (*erm*^{r})[73] or *E. coli* JW0333 (*ΔlacA783::kan*^{r}).[74] *B. thetaiotaomicron* was plated on BHI medium containing 10% horse blood (Quad Five, Cat# 210-1000), 200 μg/mL gentamicin and 25 μg/mL erythromycin. *E. coli* was plated on LB agar containing 50 μg/mL kanamycin and grown aerobically. Two-fold serial dilutions were plated for CFU determination.

Human fecal material

Human fecal material in the MV collection was obtained and prepared under the Yale University Human Investigation Committee protocol number 1106008725.[35] Briefly, donors were 20-60 years old and generally healthy based on self-report data. Material was stored in single use glycerol stock aliquots with anaerobic headspace at -80°C prior to use. The labeling of samples in a previous report[80] is the same here except samples MV26-30 in the previous study are labeled MV25-29 in the current study.

METHOD DETAILS

Chemicals

Dietary xenobiotics used in this study were purchased from MedChemExpress, Sigma, Cayman Chemicals or Santa Cruz Biosciences, and dissolved in solvents (DMSO unless otherwise indicated) to concentrations indicated in Table S1. Compound libraries for growth assays (Figure 1C), remodeling assays (Figure 2) and toxification assays (Figure 4) were arrayed in 96-well polypropylene V-bottom microplates and stored at -20°C until use.

Community remodeling and metabolism assays

Incubations to measure the metabolism of dietary xenobiotics *in vitro* were performed anaerobically. For experiments involving MV communities, glycerol stock aliquots were used to inoculate an overnight culture grown in BB:mGAM medium. For experiments involving defined communities, saturated cultures of each species were normalized based on their OD_{600} and combined. These community starter cultures were then diluted 1:50 in fresh BB:mGAM media and 400-1000 μL was dispensed into 96-well 2mL deep well plates. Each dietary xenobiotic was added to a final concentration of 10-20 μM (metabolism assays) or 200 μM (remodeling assays). Incubations were allowed to continue anaerobically for 48 hr at 37°C. Unless otherwise indicated, biological triplicate incubations were performed.

To prepare extracts for LC-MS analysis, the cultures were first mixed, then 20 μL was transferred to a 96-well polypropylene V-bottom microplate, diluted with 20 μL of acetonitrile, and vortexed briefly. Plates were centrifuged at 4000 rpm for 10 min to pellet cellular debris, then 10 μL was transferred to a new plate, diluted with 10 μL of water, and covered with a heat-sealing foil. In experiments surveying many compounds at once, as in Figures 1A, 3D, and S1B–S1D, incubations were performed independently but then pooled for LC-MS analysis. Pools were chosen so that each dietary xenobiotic and its predicted metabolites could be distinguished using orthogonal mass and retention times. Every incubation was performed in biological duplicate or triplicate alongside sterile media controls.

For community composition analysis, deep-well plates containing 400-1000 μL were centrifuged at 4000 rpm for 10 min, spent media was removed, and cell pellets were frozen at -20°C until genomic DNA extraction, as described below.

Xenobiotic metabolism by individual species

For metabolism experiments involving single species, 100 μL of a saturated culture was diluted with 100 μL of fresh media (mega media or BHI++) and 200 μL of PBS+0.05% cysteine. This setup was used for every single species measurement except for Coriobacteriial metabolism of resveratrol, which was measured in undiluted BHI++. Dietary xenobiotics were added to a final concentration of 10-20 μM and incubations were allowed to continue anaerobically for 48 hr at 37°C. Extracts for LC-MS analysis were prepared as described above.

In vitro growth assays

Starter cultures for growth assays were inoculated from frozen glycerol stocks into appropriate media (Table S2) and grown to saturation (24-48 hr). These starter cultures were then sub-cultured (1 mL into 5 mL fresh medium) and allowed to grow for a further 6-8 hr to mid-log phase. Next, 2x concentrated inoculum was prepared according to the starter OD_{600} and media conditions specified in Table S2, and 25 μL was dispensed into a 384-well plate (Thermo-scientific 12-565-342) containing 25 μL of sterile media and 1 μL of compound (10 mM stock, 200 μM final, Figure 1C) or extract (Figure 4) for a final volume of 50 μL. Sterile media and DMSO controls were included on every plate. Plates were covered with a Breathe-Easy sealing membrane and grown in Biotek Eon or Epoch2 plate readers for 24 hr without shaking. Every 15 min, the plate was mixed for 1 min prior to OD_{600} measurement. To calculate normalized growth, OD_{600} measurements were baseline subtracted and area under the curve (AUC) was integrated from 0 hr until early stationary phase, as determined by manual inspection. For the 161 compound screen (Figure 1C), AUC was normalized to the interquartile mean for all compounds, since most did not affect growth. Otherwise, AUC was normalized to DMSO controls. Technical duplicate or triplicate growth curves were performed and aberrant samples were removed by manual curation.

LC-MS analysis

Extracts from *in vitro* or *in vivo* assays were analyzed (3-4 μL) in negative mode using an Agilent 1200 Infinity UHPLC system and 6550 Q-TOF LC–ESI/MS, with an C18 Kinetex Evo column (100 mm × 2.1 mm, 1.7-mm particle size, and according guard columns, Phenomenex). The source parameters were: VCap, 3,500 V; nozzle voltage, 2,000 V; gas temperature, 225 °C; drying gas 13 l/min; nebulizer, 20 psi; sheath gas temperature 225 °C; sheath gas flow 12 l/min. A dual column set-up with alternating injection was used. LC conditions for the main pump are as follows: 0–0.5 min 0% B, 0.5–7 min 0%–70% B, 7–7.3 min 70%–95% B, 7.3–7.5 min 95% B, 7.5-7.9 min 95%–0% B, 7.9–8.5 min 0% B; A = water + 0.1% formic acid; B = acetonitrile + 0.1% formic acid; 0.4 ml min−1, 45°C). LC conditions for the reconditioning pump are as follows: 0–1.5 min 0%–95% B, 1.5–5 min 95% B, 5–6.5 min 95%–0% B, 6.5-8.5 min 0% B; A = water + 0.1% formic acid; B = acetonitrile + 0.1% formic acid; 0.4 ml min−1, 45°C). Integrated ion intensities were extracted from chromatograms using MassHunter Quantitative Analysis Software (Version B.07.01/Build 7.1.524.0 for QTOF) according to m/z and retention times listed in Table S1. Integrated ion intensities were normalized to levels in sterile media controls when possible. If a reference standard was unavailable, ion intensity was normalized to the maximum detected ion intensity in the dataset. Unless otherwise indicated, compounds labelled "parent" were added to incubations and quantified, while compounds labelled "products" were not added but were quantified.

Estimating colonic xenobiotic concentrations

To estimate physiologically relevant dietary xenobiotic concentrations likely to occur in the mammalian gut (Table S1), we adopted an approach previously used for medical drugs.[34] For each compound in our 161 dietary xenobiotic library, we determined a relevant food source, concentration in that food source (mg/100g), and typical serving size from literature references, which allowed us to calculate dose (mg). In the previous approach designed for medical drugs, 90% absorption was assumed in the small intestine.[34] However, many dietary xenobiotics are not absorbed to the same extent, and so we relied on data from ileostomy patients to estimate absorption. If this data was unavailable for a given compound, we estimated it to be similar to a structurally related compound, and if this was not available, we assumed 90% absorption as in the previous medical drug analysis.[34] Intestinal concentration was therefore estimated as the dose (in μmol) dissolved in 300 mL (approximate small intestine volume) multiplied by the ileal recovery fraction. We estimated colonic concentrations by collecting data on fecal recovery and multiplying the intestinal concentration by this fraction and a factor of 10 to account for transit time and colonic concentration, as in the previous medical drug analysis.[34] These calculations may underestimate true colonic concentrations because products from microbial metabolism are often not accounted for in ileal fluid/fecal analysis and local concentrations can exceed fecal concentration >100-fold.[81] Across 149 compounds for which we were able to gather data, the median estimated colon concentration is 398 μM (Table S1), and two-thirds of compounds were expected to reach over 200 μM in the gut (Figure S2D).

For *in silico* physiology-based pharmacokinetic modeling of intestinal concentrations, we used methods similar to those previously described.[48] The 2-dimensional structure of each dietary xenobiotic was used to calculate LogP and solubility in ADMET Predictor (version 10.4). GastroPlus (version 9.8.2) was then used to simulate intestinal levels of each xenobiotic in a 70 kg human in a fasted state after a single dose representative of a commonly consumed food. Full parameters for modelling are listed in Table S1, including colonic volume, mean precipitation time, diffusion coefficient, drug particle density, and effective permeability.

Genomic DNA extraction and 16S amplification

For genomic DNA extraction from fecal material or *in vitro* cell pellets, samples were transferred to 2 mL sterile cryotubes and resuspended in 500 μL Omega CP buffer, 250 μL SDS 20%, 550 μL phenol-chloroform isoamyl alcohol 25:24:1 and 250 μL Zirconia silica beads. The samples were lysed using a BeadBeater for 2 cycles of 2 min, centrifuged at 400 rpm at 4°C, and 100-200 μL of aqueous phase was transferred to the Omega EZ-96 Cycle Pure kit for clean-up following the manufacturers recommendations.

The V4 hypervariable region of the bacterial 16S gene was amplified and sequenced using previously published techniques.[82] Briefly, input genomic DNA was quantified (Quant-IT PicoGreen dsDNA assay kit), normalized to 5 ng/μL and amplified using barcoded primers (AccuPrime Pfx SuperMix).[83] PCR products were cleaned and normalized (Invitrogen SequalPrep kit), pooled together (384 – 432 samples), and sequenced (2x250 bp, dual 8bp indexing, 15% PhiX spike-in, Illumina MiSeq) at the Yale Center for Genome Analysis.

16S rRNA analysis

16S rRNA sequencing analysis was performed using QIIME2[75] and associated packages.[84–86] Barcodes were first extracted using QIIME v1.8. QIIME v2020.11 was used for subsequent analysis, beginning by demultiplexing using emp-paired then truncating and denoising reads using DADA2.[87] Data were inspected for quality based on the inclusion of blanks and sequence read length. Next, taxonomy was assigned using the RDP Naïve Bayesian classifier trained with NCBI Ref-Seq with the confidence cut-off of 0.7 for MV community samples and 0.4 for defined community samples. Using this confidence cut-off, 35/38 species were detectable and distinguishable in the 38-membered defined community, as listed in Table S2. Alpha- and beta-diversity measures were determined using the core-metrics-phylogenetic function at a sampling depth of 6500 for the defined community and 7000-8500 for the MV communities. This sampling depth retained >98% of samples while maintaining adequate diversity sampling, as visualized using a rarefaction curve. Aberrant replicates which may have resulted from contamination or errors in sample preparation were also identified by visual inspection of taxonomy barplots and β-diversity$_{replicates}$ and omitted from further analysis. For example, one DMSO replicate of

MV29 failed these criteria, and so only four instead of five DMSO replicates were used for this community. Bray-curtis β-diversity is reported, but weighted and unweighted-unifrac measures were also evaluated and gave comparable results (Table S3).

To determine which compounds caused significant remodeling in a community, β-diversity between replicates ($\beta\text{-diversity}_{replicates}$) was used to assess experimental and biological variation (mean of replicates μ and standard deviation of replicates σ) (Figure 2C). Compounds were considered to cause no significant disruption in a community if $\beta\text{-diversity}_{vsDMSO} < \mu+\sigma$ of $\beta\text{-diversity}_{replicates}$, or 0.24. Most compounds (93/140; 66%) did not disrupt MV20, MV29 or the defined community, validating the reproducibility of this assay. Compounds were considered to cause a significant disruption in a community if $\beta\text{-diversity}_{vsDMSO} > \mu+3\sigma$ of $\beta\text{-diversity}_{replicates}$, or 0.41. These cut-offs are marked on Figure 2C.

The relative abundance of a given taxa (class or species level, as indicated) was calculated from the feature count of that taxa in a given sample. For calculating the fold change relative abundance, taxa with <75 feature counts in a given sample were first set to 0 to account for unreliable detection. A pseudocount (0.001, or 0.1% relative abundance) was then added to the relative abundance count for each taxon to reduce noise in low abundance taxa. For the analysis of 161 dietary xenobiotics (Figure 3; Tables S4 and S5), fold change was calculated by normalizing to the interquartile mean relative abundance of that taxa in a given community across all conditions. Taxa that were only detectable in a small number of samples, and thus their interquartile mean relative abundance was 0, were considered absent for the purposes of this analysis. To calculate the fold change abundance of species in MV18 and MV20 colonized mice (Figure S7F), the relative abundance for each species at the 6 hr time point was averaged across days within a treatment window (PBS or polydatin). A pseudocount (0.001) was added to each relative abundance measure, and then the ratio between polydatin and PBS treatment windows was calculated. These ratios were calculated individually for each mouse to account for variability in the initial relative abundance of each species between mice.

Generating extracts for toxification studies

Incubations of MV or defined communities with dietary xenobiotics were performed as for metabolism/remodeling incubations, except at a final compound concentration of 500 μM and a final volume of 1 mL. Incubations with each community were performed in triplicate, and DMSO only or sterile media controls were included on every plate. Supernatant was harvested by centrifugation after 48 hr of incubation, transferred to new 96-well deep well plates, and frozen at -20°C until processing. Supernatants were brought to room temperature before extract preparation. The supernatant was acidified with 0.1% formic acid and then applied to solid phase extraction resin cartridges in a 96-well format, pre-equilibrated with water + 0.1% formic acid (HyperSep Retain PEP 30 mg/1 mL 96 Removable Well Plate). Cartridge plates were centrifuged at 600 rpm for 20 min to bind the supernatant, then washed with 1 mL of 5% methanol + 0.1% formic acid followed by centrifugation. Extracts were eluted into 96 well deep-well plates through sequential application of 500 μL methanol, 50 μL DMSO and 500 μL methanol, each followed by centrifugation at 600 rpm. Elution fractions were dried through vacuum centrifugation followed by lyophilization, and finally resuspended in 20 μL DMSO. Extraction efficiency was determined by comparing pure chemical standards to compound spiked into sterile media and extracted, followed by LC-MS quantification as described above. For each compound, we confirmed efficient extraction (>90% recovery) of the parent compound and known metabolites.

For the large-scale map generated for 94 dietary xenobiotics shown in Figures 4C and S3A, aliquots of extracts generated from triplicate incubations were pooled before testing for growth inhibition of the indicator species. If inhibitory activity was observed, the activity of each replicate was verified individually. For follow-up experiments involving all 29 MV communities (Figures 4D and 4F), duplicate incubations were performed and kept separate throughout. Importantly, incubation of compounds with sterile media, or extracts prepared from each community in the absence of any dietary xenobiotic (DMSO control), did not inhibit bacterial growth (Figure 4C).

qPCR for species and gene abundance

Genomic DNA extracted from fecal material or *in vitro* cell pellets was diluted 1:50 in nuclease free water and used as a template for qPCR using species specific primers (Table S7). To design primers specific for resveratrol reductase homologs in *Eggerthella*, *Adlercreutzia* or *Raoulibacter*, nucleotide alignments from multiple strains (listed in Figure 6C) were used to identify conserved nucleotide sequences, and specificity was tested by BLASTn. Primers were empirically verified for specificity and efficiency 85%–110% prior to use. qPCR was performed using a CFX96 instrument (BioRad) and SYBR FAST universal master mix (KAPA Biosystems). Arbitrary species abundance was calculated by 2^{-Ct} and relative abundance was normalized to the sum of the abundance of all species in a sample. Fold change abundance of each species versus DMSO was calculated for each replicate against the average relative abundance of four DMSO-treated replicates. Resveratrol reductase gene abundance was calculated by normalizing to total bacterial abundance determined using universal 16S primers.

E. lenta cell free supernatants

For cell free supernatant and RNA-seq assays, *E. lenta* was grown in basal medium containing 10 mM sodium acetate and 1% arginine, prepared as described previously.[88] For these experiments, resveratrol was dissolved in DMF instead of DMSO because DMSO serves as an electron acceptor for *E. lenta*. For cell free lysate experiments, 10 mL cultures were grown with 100 μM resveratrol or an equal volume of DMF for 24 hr. Cells were harvested through centrifugation and the cell pellet was washed twice with PBS to remove resveratrol or dihydroresveratrol from the culture. Cells were then lysed in 400 μL buffer (50 mM HEPES, 100 mM NaCl,

0.05% cysteine, pH 7.3) by bead beating with Zirconia silica beads. Lysates were centrifuged and the supernatant was harvested. Protein content was normalized to 20 μg/mL using a Bradford assay, and finally 100 μM resveratrol (dissolved in DMSO) was added in 100 μL reaction volumes. All steps until this point were performed anaerobically. These reactions were then incubated either aerobically or anaerobically at 37°C for 24 hr, quenched with 100 μL acetonitrile + 0.5% formic acid, and analyzed by LC-MS.

E. lenta RNA-seq

E. lenta was inoculated from a single colony and grown in basal medium for 48 hr. This culture was diluted 1:10 into 10 mL fresh medium and grown to an OD_{600} of 0.2 (24-26 hr), in triplicate. Resveratrol (100 μM) or an equal volume of DMF was added to these cultures and grown to an OD_{600} of 0.5 (6-8 hr). Cells were harvested by centrifugation, washed with RNAprotect (Qiagen 76506), and frozen at -80°C until processing. Crude RNA was extracted by bead beating in 1 mL TRIzol (Thermofisher) using Zirconia silica beads (2 cycles x 2 minutes), followed by addition of 200 μL chloroform and centrifugation at 4°C for 10 min. The aqueous phase was recovered and mixed with an equal volume of 100% ethanol. RNA was further purified using the RNeasy mini kit (Qiagen 74106) according to the manufacturer's instructions. 10 μg of purified RNA was treated with DNAse using the Ambion DNA-free kit, and subsequently cleaned using RNeasy spin columns (Qiagen). Bacterial rRNA depletion was performed using the NEBNext rRNA Depletion Kit and libraries were prepared using the NEB Ultra II Directional Library Prep Kit for Illumina. Sequences was performed on an Illumina NovaSeq (2x100bp, 35 million reads/sample) at the Yale Center for Genomic Analysis.

For analysis, reads were aligned to the *E. lenta* DMS 2243 reference genome (Genbank accession GCF_000024265.1) using Bowtie2 (v2.4.2).[76] Gene counts were determined with featureCounts in Rsubread (v2.14.2; isPairedEnd=TRUE, countReadPairs=TRUE)[77] and these data were used to calculate RPKM. Volcano plots were generated using DESeq2 (v1.40.1)[78] with cut-offs set at $p_{adj} < 0.01$ and $\log_2$(fold change) > 2. The upregulation of *Elen_288* and *Elen_1284* was independently verified using qRT-PCR.

Coriobacteriia genetic manipulation

Tools for genetic manipulation of *E. lenta* and *G. urolithinfaciens*, including pXD68Kan2-AphA and pXD71Cas10RFP-Pct5.1-crRNA(AarI)-RFP,[61] were a gift from Emily Balskus. *E. lenta* CRISPR mutants were generated using pXD71-Cas10.1 with the primers listed in Table S7 using methods similar to previously described.[61] Protospacer targets of the form TTC-N_{34} were selected in genes of interest and incorporated into oligonucleotides of the form AAAT-N_{34} and TGAC-N_{34}. These oligonucleotides were mixed, annealed, and phosphorylated using T4 polynucleotide kinase, then cloned into pXD71Cas10RFP-Pct5.1-crRNA(AarI)-RFP via Golden Gate assembly with the restriction enzyme PaqCI. Homology repair templates were designed to create clean gene deletions and flanked ~1 kb upstream and downstream of the targeted gene (Figure S6A). Homology arms were amplified from *E. lenta* genomic DNA and cloned into PCR-amplified pXD71Cas10 backbone (containing CRISPR RNAs; crRNAs) via Gibson assembly, generating pXD71Cas10-crRNA-288 targeting *Elen_288*, or pXD71Cas10-crRNA-1283-5, targeting the operon *Elen_1283-5*. These constructs were transformed into *E. lenta* via electroporation, as previously described,[61] and plated on BHIrf plates supplemented with kanamycin (100 μg/mL). After 3-4 days, colonies were inoculated into BHIrf broth with kanamycin and cumate (50 μM) to induce expression of crRNA. At this point, diagnostic primers binding outside of the homology repair template region were used to check for successful genome editing events (Figure S6B). In colonies where both wildtype and edited band sizes were detectable, the cultures were re-streaked on BHIrf+kanamycin+cumate to ensure full removal of the wildtype gene. We were unable to introduce a complementation construct (pXD70Tet(LacZ3)[61]) into CRISPR engineered *E. lenta* strains, possibly owing to incompatibility with pXD71Cas10 in these strains.

Divergently encoded from *Elen_288* is a 12-transmembrane spanning LuxR family transcriptional regulator, *Elen_289*, which belongs to a gene family in Coriobacteriia previously shown to specifically respond to and regulate catechol dehydroxylase gene expression.[61] For expression of *Elen_288* and *Elen_289* in *G. urolithinfaciens*, the native gene cassette spanning *Elen_288* to *Elen_289* was amplified from *E. lenta* using primers listed in Table S7. Linear vector backbone was PCR amplified from pXD68Kan2-AphA,[61] removing the YFP cassette from this construct, and *Elen288-289* was inserted via Gibson Assembly. This construct, pXD68-288-289, or the original construct, pXD68Kan2-AphA, were transformed into *G. urolithinfaciens* as previously described,[61] and plated on BHIrf plates supplemented with kanamycin (100 μg/mL). After 3-4 days, transformants were verified by colony PCR and metabolism was assayed.

Analysis of Elen_288 homologs

Coriobacteriial genomes were collated, including 79 genomes previously collected that span 20 different genera,[89] 14 additional *Adlercreutzia* genomes, and 3 additional genomes identified from RefSeq that contain an *Elen_288* homolog. *Bifidobacterium animalis* was included as an outgroup. A homolog to *Elen_288* in *A. equolifaciens* (*Aqeu_2118*, with 76.3% amino acid identity) was first identified and verified by phenotypic evidence. Homologs in the other 95 coriobacteriial genomes were identified with tBLASTn using Elen_288 or Aequ_2118 protein sequences as queries. Notably, *Gordonibacter pamelaeae*, *G. urolithinfaciens* and *Slackia isoflavoniconvertens*, which cannot metabolize resveratrol (Figure S4C) encode only distant homologs (<42% amino acid identity). Therefore, an amino acid identity cut-off of 70% was selected since it effectively identified homologs that could be verified through reciprocal BLAST, removed paralogs of Elen_288 encoded elsewhere in the *E. lenta* DSM2243 genome, and removed hits in non-metabolizing species. These homologs were mapped onto a phylogenetic species tree built using CodonTree on PATRIC,[90] ultimately using an alignment of 16 conserved CDS, 6085 amino acids, or 18255 nucleotides to generate the tree shown.

Metabolism of dietary xenobiotics in mice

Germfree mice were colonized with MV communities by gavaging 100 μL of human fecal material (preserved in glycerol and stored at -80°C with anaerobic headspace, as described above) and allowing the community to stabilize for 7 days. Each group contained 3-5 mice as indicated in figure legends. In general, dietary xenobiotics were dissolved in PBS and <5% DMSO, mice were gavaged with 100-200 μL, samples were collected at the indicated time points in sterile 2.0 mL screw cap tubes, and tubes were flash frozen in liquid nitrogen. Timing of gavage was staggered to allow for precise collection time points. For measuring the colonic concentration of common dietary xenobiotics in germfree mice (Figure S2B), a pool of dietary xenobiotics (polydatin, myricitrin, narirutin, hesperidin, quercitrin, genistin, phlorizin, EGCG, chlorogenic acid, rebaudioside A, and neotame) was gavaged at 10 mg/kg in 200 μL, mice were sacrificed 4.5 hr post-gavage, and intestinal contents was collected. For measuring metabolism in mice colonized with four MV communities (Figure S4A), a pool of dietary xenobiotics (hesperidin, polydatin, rebaudioside A) was gavaged at 40 mg/kg in 200 μL, mice were sacrificed 4.5 hr post-gavage, and intestinal contents was collected. Rebaudioside A was used in these experiments instead of stevioside for cost considerations. In all experiments measuring the metabolism of resveratrol by different defined or MV communities (Figures 7 and S7), polydatin was gavaged at 30 mg/kg in 100 μL at 0hr, 3hr and 6hr, and fecal pellets were collected at 6 hr or 9 hr post-gavage.

To prepare extracts for LC-MS analysis, intestinal material or fecal pellets were weighed (~20-100 mg), then extracted with 400 μL of actetonitrile/methanol (1:1, ice cold) with 10 μM urolithin C, used as an internal standard for LC-MS detection. Samples were bead beat with Zirconia silica beads for 2 min and centrifuged (10 min, 4000 rpm, 4°C) to remove debris. Supernatant was transferred to clean tubes, centrifuged again to remove remaining debris, then diluted 1:5 in water for LC-MS analysis. To prepare serum samples for LC-MS analysis, 10 μL serum was combined with 40 μL acetonitrile/methanol (1:1, ice cold), placed at -20°C for 1 hr, then spun down and supernatant transferred to a new plate. Standard curves were prepared in parallel by spiking reference standards into germfree cecal material or serum at appropriate concentrations (0.1-1000 μM). To calculate concentration in fecal matter, integrated ion intensity was normalized to the weight of the extracted sample and compared to this standard curve.

Remodeling of microbial communities in mice

For defined communities, saturated cultures of each species were normalized based on their OD_{600} and mixed together (Base community: *E. coli, E. cancerogenes, B. thetaiotaomicron, A. muciniphila, B. adolescentis, C, scindens, C. sporogenes, E. rectale, R. gnavus*; Additionally: *E. lenta* and *E. ramulus*). *E. ramulus* was also included in the *E. lenta* community but colonized at <0.1% and ultimately did not affect the outcome of this experiment. Mice were colonized with each defined community or human community, 3-5 per group as indicated, and community composition allowed to stabilize for 7 days. At this point, mice were dosed daily with vehicle (95 μL PBS, 5 μL DMSO), or 30 mg/kg polydatin (95 μL PBS, 5 μL 6.25 mg/mL polydatin in DMSO) at 0 hr, 3hr and 6hr time points. Fecal samples were collected at 0 hr, 6 hr and 9 hr time points. For the defined community experiment (Figures 7A–7C), PBS treatment continued for 5 days, followed by 2 days recovery, and 5 days of polydatin treatment. For the human community experiment (Figures 7E–7G), PBS treatment continued for 2 days, followed by 2 days recovery, and 3 days of polydatin treatment. Fecal pellets collected were analyzed for community composition (qPCR, 16S sequencing) and LC-MS analysis.

QUANTIFICATION AND STATISTICAL ANALYSIS

Statistical analysis was performed using GraphPad Prism 9. Details of statistical tests used, sample size indicated as ''n'', definition of means, error bars, and significance are provided in figure legends. Tukey's post-hoc analysis was used in most cases. Bonferroni's post-hoc analysis was used when the number of comparisons was small, and Dunnett's post-hoc analysis was used when comparison to a single control group was made. Figures were generated in GraphPad Prism 9 and in Tibco Spotfire 6.5.1.

Supplemental figures

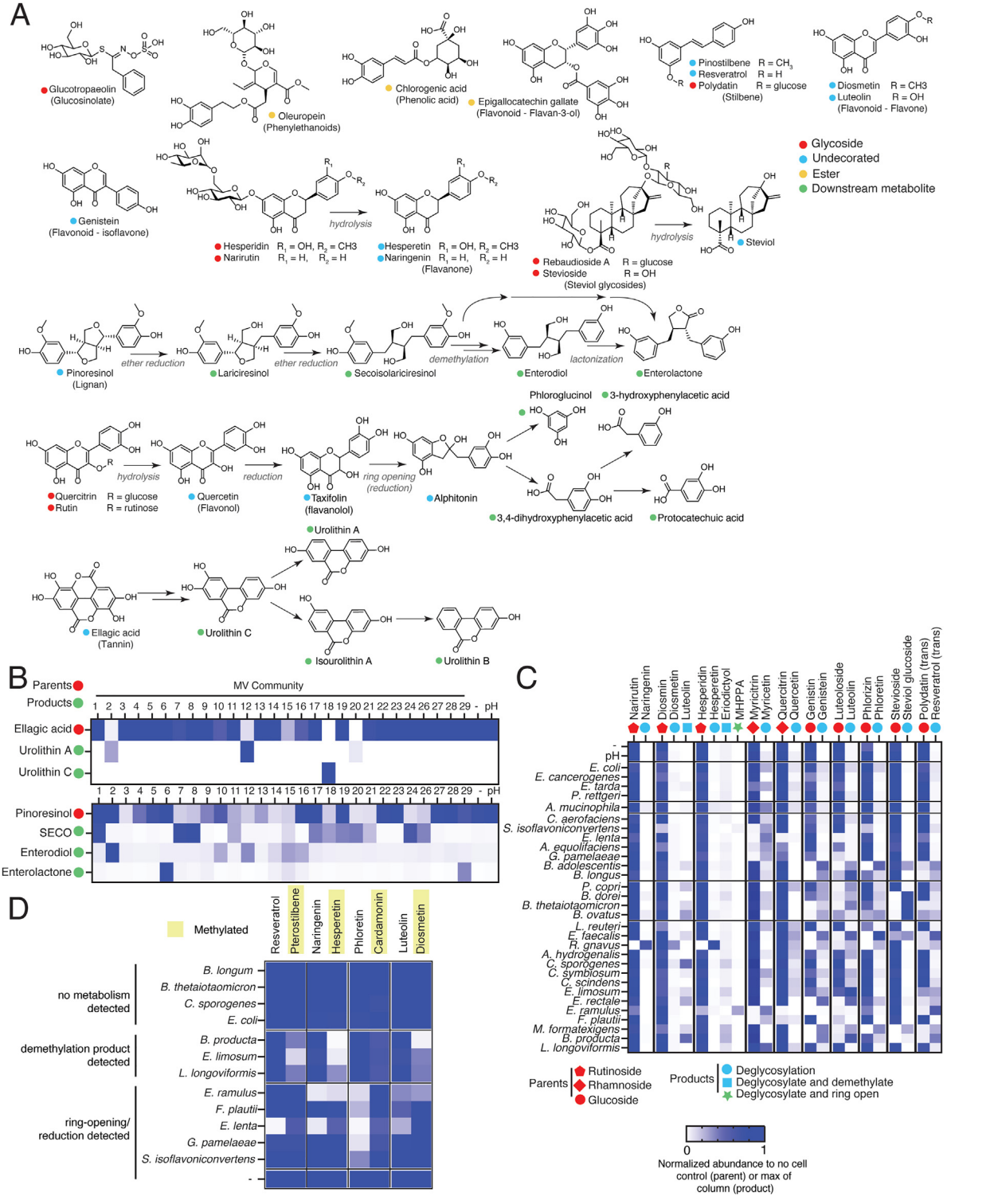

(legend on next page)

Figure S1. Metabolism of dietary xenobiotics by the gut microbiome, related to Figure 1

(A) Structures and metabolic pathways for compounds included in Figure 1A. Colored shapes are used to denote different forms of parent compounds and metabolites.

(B–D) Heatmaps representing the metabolism of dietary xenobiotics. Parent compounds are added to incubations, and then the disappearance of parents and the appearance of products are quantified by LC-MS. Abundance is normalized to no-cell control (for parent compounds) or to the maximum value in the column (for products). (B) Metabolism of the tannin ellagic acid and the lignan pinoresinol through different metabolic pathways (A) across 29 human fecal communities. Pinoresinol is metabolized to secoisolariciresinol, enterodiol, or enterolactone by different communities,[91,92] while ellagic acid is metabolized to urolithins A or C.[93,94] (C) Metabolism of 10 different dietary glycosides (parent compounds) by 30 human gut bacterial species. (D) Metabolism of structurally related compounds that differ in methoxyl decoration, indicated by yellow shading. Compound pairs exemplifying this relationship include the flavones diosmetin (4′-methoxyl; largely non-metabolized) vs. luteolin (widely metabolized), the flavanones hesperetin (4′-methoxyl) vs. naringenin, the stilbenes pinostilbene (3′-methoxy) or pterostilbene (3′,5′-dimethoxy) vs. resveratrol, and the chalcones cardamonin (6′-methoxy) vs. phloretin. Three species (*Blautia producta*, *Eubacterium limosum*, and *Lactonifactor longoviformis*; all acetogens marked by asterisks) have the capacity to demethylate these substrates. MHPPA, 3-(4-methoxy-3-hydroxyphenyl)propionic acid. In (B)–(D), "-" indicates the sterile media control and pH indicates the pH 5 control.

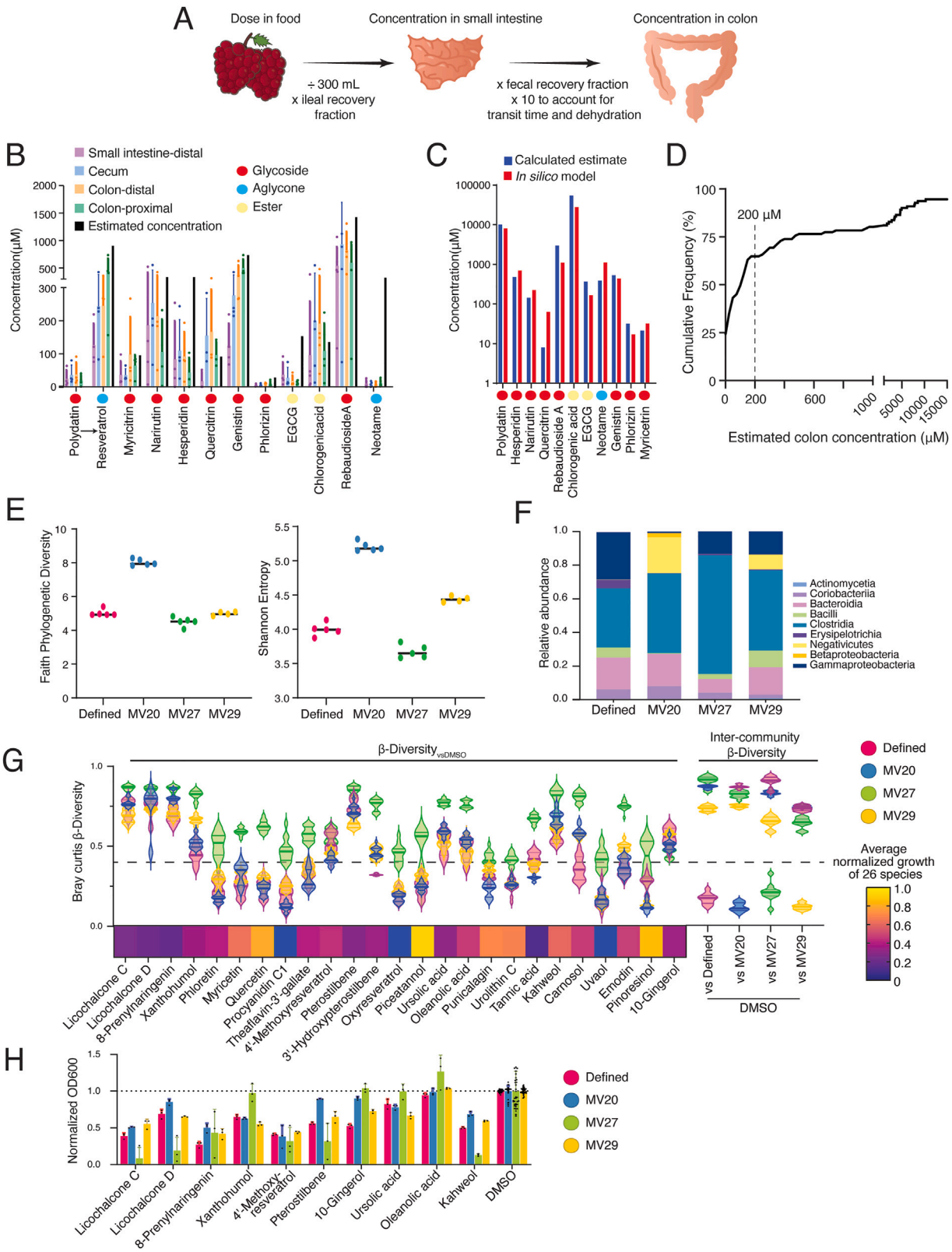

(legend on next page)

Figure S2. Physiologically relevant concentrations of dietary xenobiotics remodel the gut microbiome *in vitro*, related to Figure 2

(A) Strategy for calculating the colonic concentrations of dietary xenobiotics. See also Table S1.

(B) Measured colonic concentrations of 11 different dietary xenobiotics in germfree mice after a single 10 mg/kg dose. Mean and standard deviation are shown (n = 4 mice). Estimated concentrations are calculated using the method shown in (A) and Table S1, based on a dose of 10 mg/kg and with allometric scaling for mice. Note that polydatin is transformed into resveratrol in these mice, as indicated by the arrow.

(C) Estimated colonic concentrations of the same 11 dietary xenobiotics in humans after a single dose in a commonly consumed food. Calculated estimates (as in A; blue) and results from *in silico* physiology-based pharmacokinetic modeling (red) are shown. All doses and parameters are listed in Table S1.

(D) Estimated human colonic concentration of 149 dietary xenobiotics from typical food portions, plotted against cumulative frequency. See also Table S1.

(E and F) (E) Alpha-diversity measures and (F) community composition for MV20, MV27, MV29, and the 38-member defined communities treated with DMSO. Mean is shown (n = 5 biological replicates except for MV29, n = 4).

(G) Summary of 25 dietary xenobiotics that significantly remodel at least 1 of the 4 tested communities ($\beta\text{-diversity}_{\text{vs. DMSO}} > 0.41$). β-diversity is represented as a violin plot and indicates distances either between dietary xenobiotic and DMSO treatments of the same community ($\beta\text{-diversity}_{\text{vs. DMSO}}$), or two different communities both treated with DMSO (inter-community β-diversity). Mean and standard deviation are shown (n = 15). Toxicity is represented as a heatmap, where normalized growth of 26 species (Figure 1C) is averaged.

(H) OD_{600} normalized to DMSO controls of the MV20, MV27, MV29, and 38-member defined communities incubated with 10 pan-disruptive compounds at 200 μM.

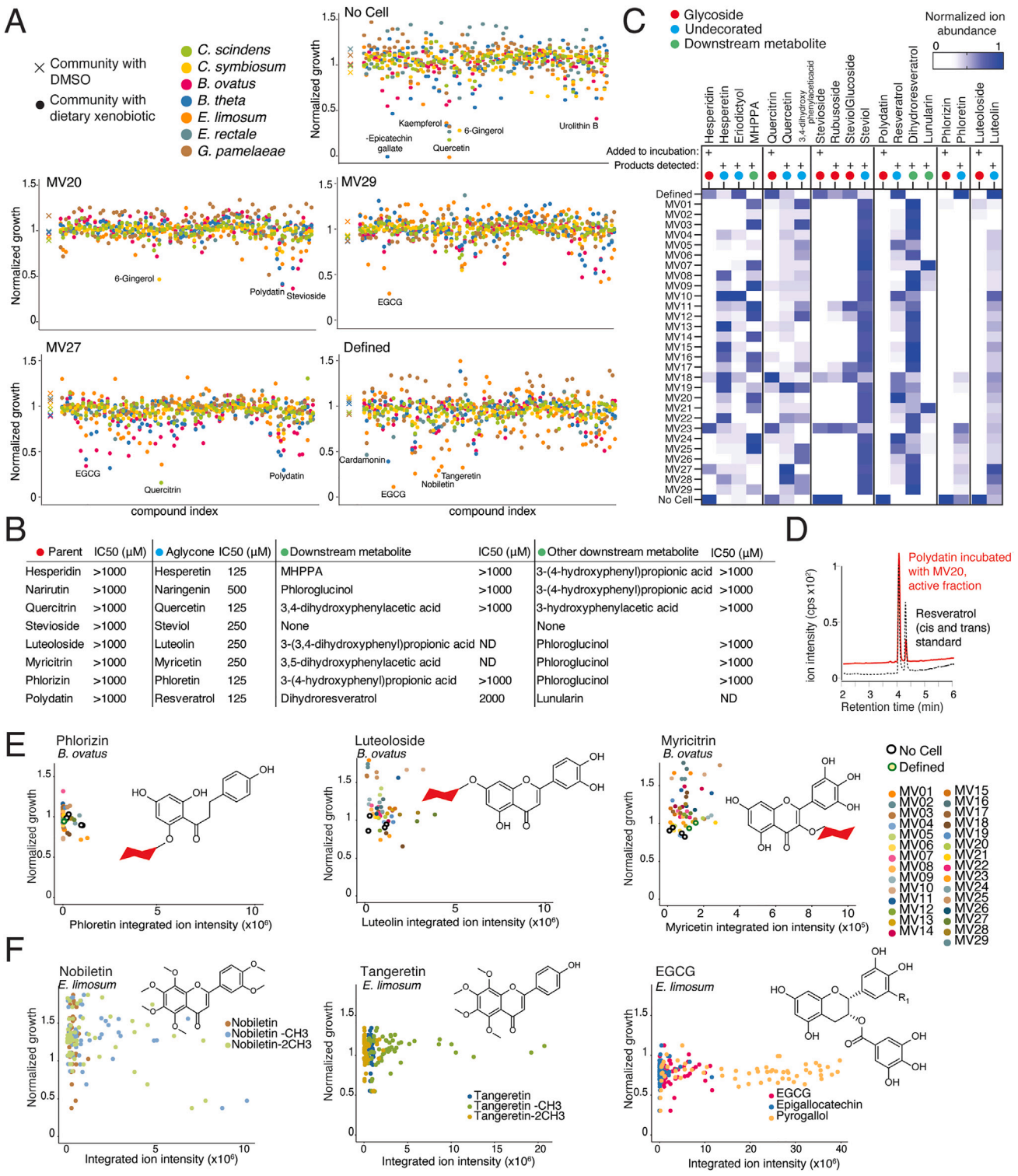

Figure S3. Microbial metabolism can toxify dietary xenobiotics, related to Figure 4

(A) Normalized growth of 7 indicator species (colored dots) in the presence of extracts prepared from incubation of 94 dietary xenobiotics (indexed along the x axis) with four different microbial communities and a no-cell control. Compounds that are toxic to at least one indicator species without community incubation are labeled in the no-cell control plot, whereas points labeled in the other plots indicate compounds that become toxic after incubation with a community. Each point represents the mean of two independent growth measurements, and growth is normalized to DMSO controls.

(legend continued on next page)

(B) Inhibitory concentrations (50% growth; IC_{50}) of parent glycosides, their aglycone forms, and downstream metabolites. The indicator species is *E. limosum* for polydatin and its metabolites and *B. ovatus* for all other compounds. See also Figure 4D.

(C) Heatmaps representing the metabolism of dietary xenobiotics by 29 human communities. Parent compounds are added to incubations, and then disappearance of parent and appearance of products are tracked. Ion abundance is normalized to the sterile media control (for parent compounds) or maximum of the column (for product compounds).

(D) Activity-guided purification of the inhibitory compound produced by incubation of polydatin with community MV20. LC-MS total ion chromatogram of the inhibitory fraction isolated is shown, alongside a resveratrol reference standard (two peaks represent *cis* and *trans* isomers).

(E and F) Relationship between normalized growth of *B. ovatus* or *E. limosum*, as labeled, and detection of toxic aglycones (E) or other predicted metabolites (F) in extracts prepared from the parent compounds labeled in the top left of each graph. In (E), each of these three dietary xenobiotics is fully detoxified and metabolized, indicated by low detection of the toxic aglycones. Different colors represent different communities, as indicated in the figure legends. In (F), detection of predicted metabolites does not correlate with growth inhibition. Different colors represent the detection of different metabolites, as indicated by the figure legends. For ion abundance data in (B), (E), and (F), individual replicate incubations are shown ($n = 1$). For normalized growth in (E) and (F), mean of two independent extract preparations followed by two independent growth measurements ($n = 4$) is shown.

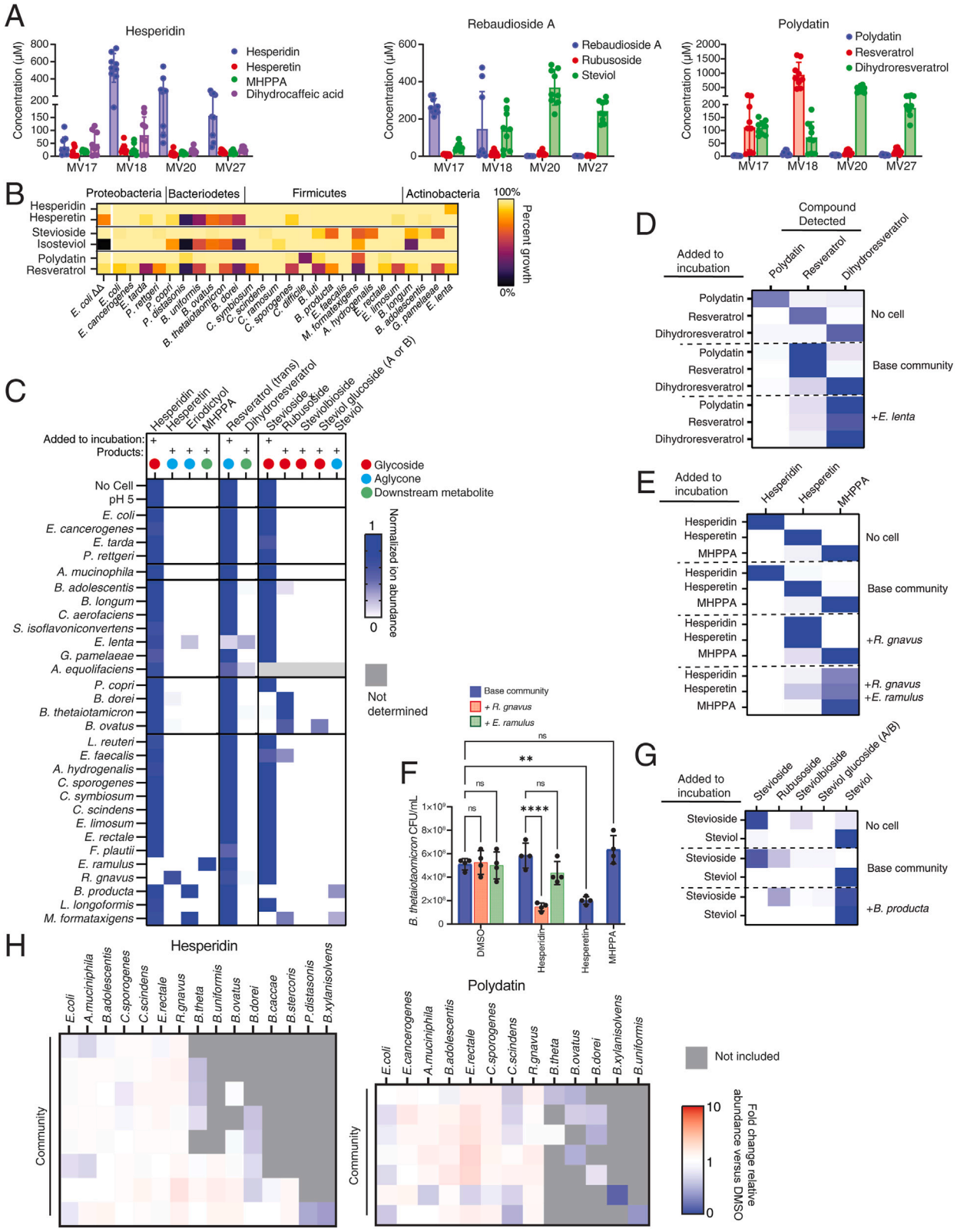

(legend on next page)

Figure S4. Mechanistic studies on community remodeling by hesperidin, polydatin, and stevioside, related to Figure 5

(A) Metabolism of hesperidin, polydatin, and rebaudioside A (related to stevioside) in ex-germfree mice colonized with four different human microbiome communities. Parent compounds and microbial metabolite concentrations, averaged across the cecum and proximal colon, were measured. Mean with standard deviation are plotted (n = 3 mice/group × 3 measurements/mouse = 9).

(B) Normalized growth of 26 gut commensals in the presence of select compounds and their toxic aglycones. See also Figure 1C.

(C) Heatmaps representing the metabolism of key compounds by individual species. Parent compounds are added to incubations, and then disappearance of parent and appearance of products are tracked. Abundance is normalized to no-cell control (for parent compounds) or to the maximum value in the column (for products).

(D, E, and G) Heatmaps representing the metabolism of key compounds by 8–10 membered defined communities. Compounds added to the incubations are labeled on the left, and detected compounds are along the top. Additional species added to base communities are labeled on the right. See also Figures 5B (relates to D), 5D (relates to E), and 5F (relates to G).

(F) Absolute abundance of *B. thetaiotaomicron* (*Δtdk att1::pNBU2-BC1*[73]) measured via CFU plating. Significance is calculated using two-way ANOVA with Tukey's post hoc analysis (n = 4; $^{**}p$ = 0.0024, $^{****}p < 0.0001$).

(H) Heatmaps representing fold change relative abundance of species in a defined community treated with hesperidin or polydatin compared with DMSO controls. *Bacteroides* spp. included in each community are shown at right. For all heatmaps (B–E, G, and H), mean of four biological replicates is shown (n = 4).

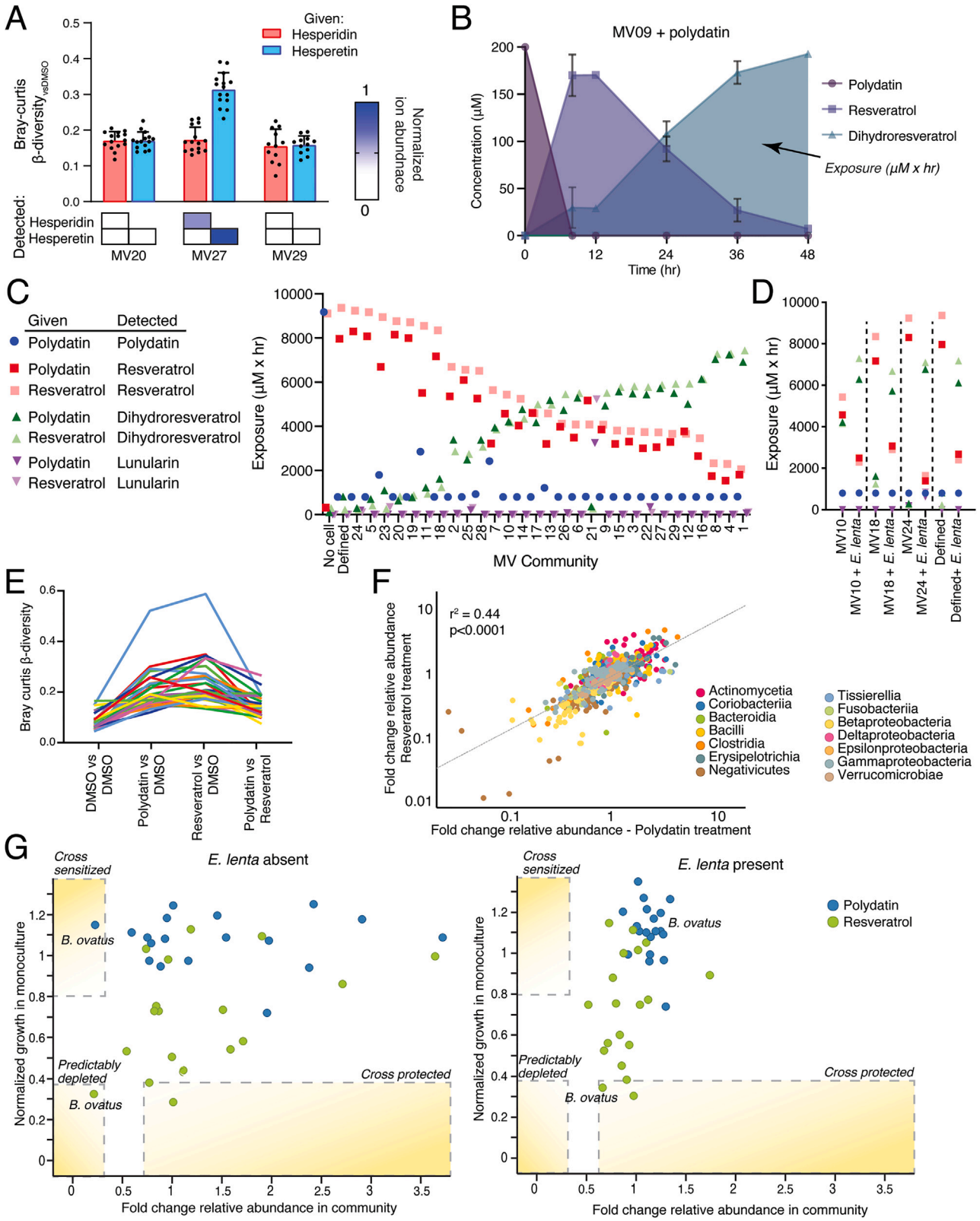

(legend on next page)

Figure S5. Complex communities are remodeled *in vitro*, related to Figure 5

(A) Metabolism is related to β-diversity$_{vs.\ DMSO}$ for three MV communities after application of either hesperidin or hesperetin, as in Figures 2 and S2. Detection of hesperetin in culture media, normalized to levels in sterile media, is shown in the heatmap at the bottom. Hesperetin was only detected in the incubation of MV27 with hesperetin, and only this community had an elevated β-diversity$_{vs.\ DMSO}$ in response to hesperetin exposure. Heatmap shows mean of triplicate incubations and mean and standard deviation of β-diversity$_{vs.\ DMSO}$ is plotted (5 DMSO replicates × 3 hesperidin/hesperetin replicates = 15).

(B) Representative time course of metabolism of polydatin by a human gut community (MV09), as determined across 6 time points by LC-MS. The shaded area under the curve illustrates how exposure was calculated. Mean and standard deviation of three independent incubations are shown.

(C and D) Exposure of MV communities to polydatin and resveratrol. Either polydatin or resveratrol was given to the community, and detected metabolites are indicated. Lunularin is a dehydroxylated form of dihydroresveratrol. *E. lenta* is variably added to communities in (D), resulting in enhanced resveratrol metabolism.

(E) β-Diversity between DMSO, polydatin, and resveratrol treatments of 25 human gut microbiome communities *in vitro*, as indicated by different colored lines. The mean β-diversity between two compounds with three replicates each is shown (DMSO vs. DMSO: $n = 3$; polydatin/resveratrol vs. DMSO or polydatin vs. resveratrol: $n = 3 \times 3 = 9$).

(F) For each of the 25 human communities, the fold change relative abundance (compared with DMSO) of each bacterial class after resveratrol treatment is correlated to its change after polydatin treatment. Pearson correlation is shown.

(G) Response of the defined community treated with either polydatin or resveratrol, similar to Figure 3C. The community consists of 37 or 38 members, depending on *E. lenta* addition as indicated. Normalized growth in monoculture of each species treated with the given compound (from Figure 1C) vs. fold change relative abundance (compared with DMSO) in the community is plotted. Interactions with *B. ovatus* that demonstrate cross-sensitization and cross-protection are labeled. In (F) and (G), mean fold change relative abundance in triplicate incubations is shown.

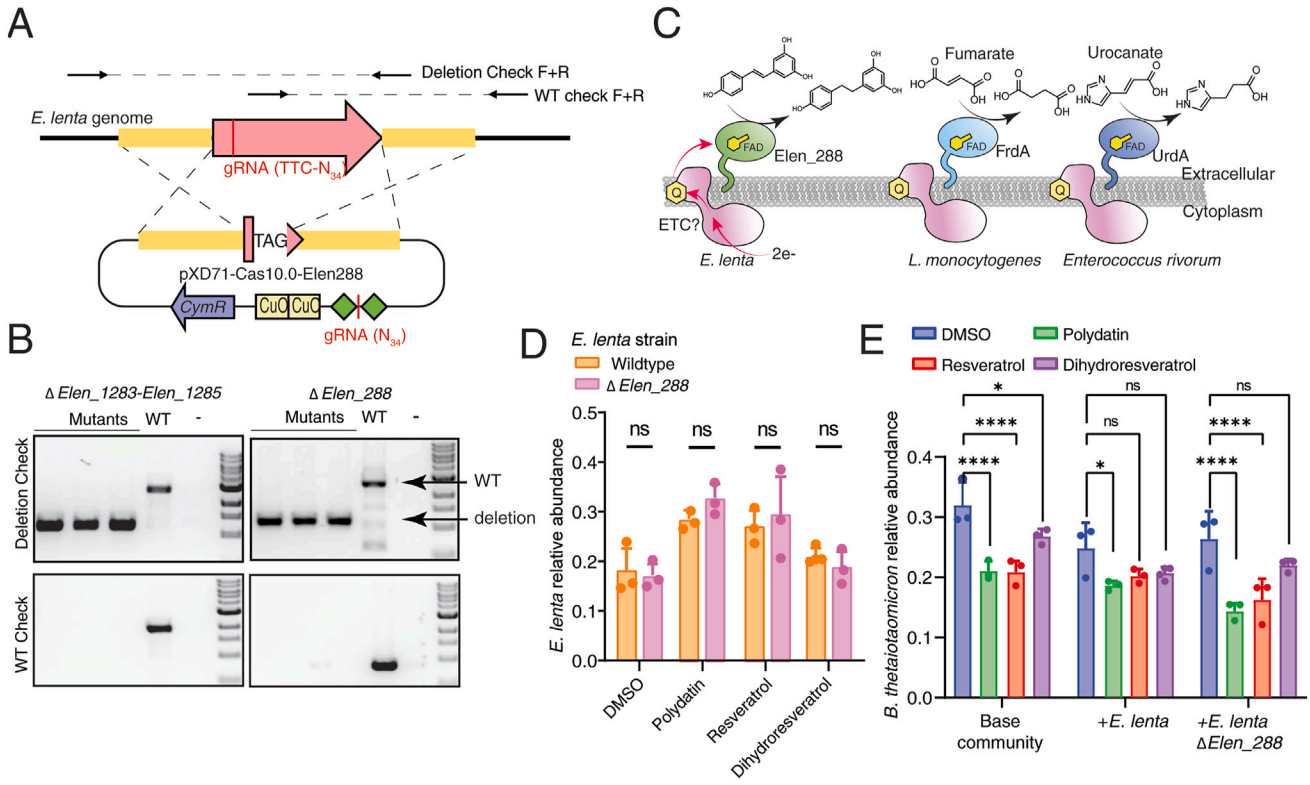

Figure S6. Generating a CRISPR mutant of *Elen_288*, related to Figure 6

(A) Schematic for clean deletion of targeted genes by homologous recombination using CRISPR-targeting plasmid pXD71-Cas10.0.[61] Expression of the crRNA is controlled by a cumate inducible system consisting of the repressor CymR and operator sequences CuO. The relative location of primers used to validate mutants is indicated.

(B) Validation of *E. lenta* mutants by PCR. PCR products from three different mutants are shown alongside wild-type *E. lenta*.

(C) Schematic showing proposed function of Elen_288 and its analogous functions in *L. monocytogenes* and *E. rivorum*. Membrane quinone pools, indicated by "Q," shuttle electrons as part of the electron transport chain. It is proposed that these quinones pass electrons to flavin adenine dinucleotide (FAD) cofactors in Elen_288, FrdA, or UrdA.[62]

(D and E) Relative abundance of *E. lenta* strains (D) or *B. thetaiotaomicron* (E) in 9–10 membered defined communities, similar to Figure 5B. *B. thetaiotaomicron* levels are quantified in defined communities variably including *E. lenta* strains, as indicated. *E. lenta ΔElen_288* fails to protect *B. thetaiotaomicron* from depletion by polydatin or resveratrol. Mean and standard deviation of biological replicates are shown ($n = 3$). Significance is tested by two-way ANOVA with Dunnett's post hoc analysis. *$p < 0.05$, ****$p < 0.0001$.

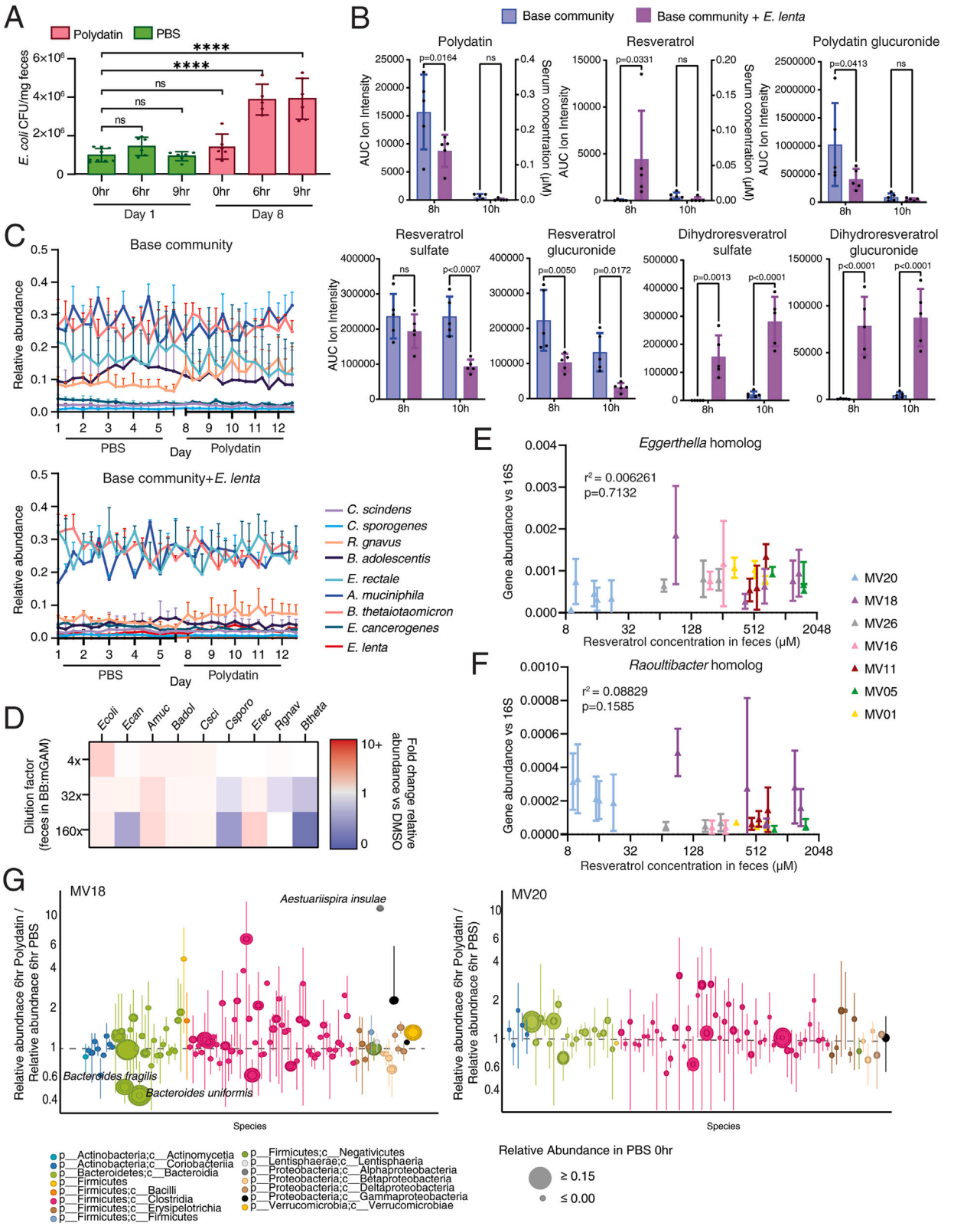

(legend on next page)

Figure S7. Polydatin metabolism predicts community remodeling *in vivo*, related to Figure 7

(A) Absolute abundance of *E. coli* in mice colonized by the 9-member defined community lacking *E. lenta* during PBS (day 1) or polydatin (day 8) treatment as in Figure 7A. Significance is calculated using one-way ANOVA with Dunnett's post hoc analysis ($n = 5$ mice, $^{****}p < 0.0001$).

(B) Serum levels of polydatin and its metabolites in mice colonized with defined communities, including or lacking *E. lenta*, and dosed as in Figure 7A. Serum metabolites were measured 8 and 10 h after the first gavage. Concentrations were quantified for polydatin and resveratrol using authentic standards and plotted on the right y axes. Arbitrary area under the curve (AUC) ion intensities are shown for all other compounds. *p* values were calculated by two-way ANOVA with Sidak's multiple comparison analysis ($n = 5$).

(C) Relative abundance of species in mice colonized by a defined community during PBS and polydatin treatment. All species are shown except for *E. coli*, which is shown in Figure 7C. Mean and standard deviation from 3 to 5 replicate mice are shown (base community: $n = 5$, base community + *E. lenta*: $n = 3$).

(D) Heatmaps representing fold change relative abundance after *ex vivo* incubation of fecal material treated with 500 μM resveratrol vs. DMSO. Fecal pellets were collected from mice colonized with the base-defined community lacking *E. lenta*, as in (A), and diluted in Bryant and Burkey Medium:Modified Gifu Anaerobic Medium (BB:mGAM media). Mean of three biological replicates is shown ($n = 3$).

(E and F) Relationship between resveratrol metabolism in ex-germfree mice and gene abundance of resveratrol reductase homologs in either *Eggerthella* (E) or *Raoultibacter* (F). Resveratrol was measured in feces at the 9 h time point after dosing using the scheme in Figure 7A. Each point represents an individual mouse ($n = 3$–5 mice per MV community, as shown). Mean and standard deviation in gene abundance are shown from samples collected from 4 different days ($n = 4$). Pearson correlation coefficients were calculated.

(G) Fold change relative abundance of species in MV18- or MV20-colonized mice during polydatin treatment compared with PBS treatment. y axis shows a log scale. Mean and standard deviation for replicate mice are shown ($n = 5$).